2019 BES Geosciences PI Meeting
6-8 Aug 2019
Marriott Washingtonian Hotel
Gaithersburg, MD

Overview

Tues 6th		**Wed 7th**		**Thu 8th**	
7:30	BREAKFAST	8:00	BREAKFAST	7:00	BREAKFAST
8:15	**Rustad** BES				
8:30	**Garrett** BES				
9:00	**Ilton** PNNL	9:00	**Shaw** UArk	8:00	**Ben-Zion** USC
9:30	**Harvey** TxsChrstn	9:30	**Misra** UOklhm	8:30	**Zhu** UMd
10:00	**Lee** ANL	10:00	**Carey/Viswanathan** LANL	9:00	**Brodsky** UCSntCrz
10:30	BREAK	10:30	BREAK	9:30	BREAK
10:45	**Navrotsky** UCDvs	10:45	**Martinez-Lorenzo** NEU	9:45	**Eiler** Caltech
11:15	**Min** UCIrvn	11:15	**Ladd** UFlrda	10:15	**Kavner** UCLA
11:45	**Stubbs** UChcg	11:45	**Juanes** MIT	10:45	**Tripati** UCLA
12:15	LUNCH	12:15	LUNCH	11:15	ADJOURN
1:30	**Rundle** UCDvs	1:30	**Werth** UTxsAstn		
2:00	**Shokouhi** PSU	2:00	**Criscenti** SNL		
2:30	**Shirzaei** UArzna	2:30	**Stack** ORNL		
3:00	BREAK	3:00	BREAK		
3:15	**Buscarnera** NWU	3:15	**Sitchler** ClrdSchlMns		
3:45	**Wenk** UC Brkly	3:45	**Bourg** Prnctn		
4:15	**Pyrak-Nolte** Prdu	4:15	**Cole** OhioStU		
4:45	BREAK	4:45	BREAK		
5:00	**Johnson** LANL	5:00	**Lammers** LBNL		
5:30	**Johnson/Pyrak-Nolte**				
6:00	DINNER (provided)				
7:15	**Dixon** UAlbma	7:30	**Yuen** Clmbia		
8:30	Poster I	8:00	Poster II		

Program

Tuesday Morning

7:30 Breakfast

8:15 **Jim Rustad**, BES, Welcome
8:30 **Bruce Garrett**, BES, BES/CSGB Update

Session I, Chair: Kevin Rosso, PNNL

9:00 **Eugene Ilton**, Pacific Northwest National Lab
Incorporation of Metal Impurities in Fe(III) (Oxyhydr)Oxides

9:30 **Omar Harvey**, Texas Christian University
Probing Dynamics of Mineral-Organic Interactions using Real-time, High Temporal Resolution Energetics

10:00 **Sang Soo Lee**, Argonne National Lab
Multivalent Cation Adsorption on a Charged Mineral-Water Interface

10:30 Break

Session II, Chair: Trish Dove, VA Tech

10:45 **Alex Navrotsky**, UC Davis
Materials of the Universe

11:15 **Younjin Min**, UC Irvine
Influence of Nanoconfinement on Interactions and Relaxation Dynamics of Geocolloids

11:45 **Joanne Stubbs**, University of Chicago
Next-Generation Synchrotron X-ray Methods and Tools for Quantifying Complexity at Mineral-Fluid Interfaces

12:15 Working Lunch

Tuesday Afternoon

Session III, Chair: Bertrand Rouet-LeDuc, LANL

1:30 **John Rundle**, UC Davis
Constrained Inversion Percolation Model: Growth via Leath Bursts and the Origin of Seismic b-Value

2:00 **Parisa Shokouhi**, Penn State University
Coupled Assessment of Seismic, Hydraulic, and Frictional Properties of Fractured Rock to Illuminate Fundamental Processes Governing Energy Production and Waste Storage

2:30 **Manoocher Shirzaei**, Arizona State
New Advances in Physics-Based Induced Earthquake Forecasting

3:00 Break

Session IV, Chair: Steve Laubach, U Texas Austin/BEG

3:15 **Giuseppe Buscarnera**, Northwestern
Breakage and Creep in Wet Granular Solids: from Grain Fracture to Strain Localization

3:45 **Rudy Wenk,** UC Berkeley
Residual lattice strain in quartzites as a paleopiezometer

4:15 **Laura Pyrak-Nolte,** Purdue
Chattering Dust & Architected Fracture Networks

4:45 Break

5:00 **Paul Johnson,** Los Alamos National Lab
Probing Fracture and Fault Physics with Machine Learning

5:30 **Paul Johnson** and **Laura Pyrak-Nolte**
Kaggle Report

6:00 Dinner (provided)

Tuesday Evening

7:15 **David Dixon,** University of Alabama
Computational Geochemistry: Reliably Moving to Solution & the Bulk

8:30 **Poster Session I**

Wednesday Morning

8:00 Breakfast

Session V, Chair: Jens Birkholzer, LBNL

9:00 **John Shaw,** University of Arkansas
Structure and Dynamics of Branching and Looping Channels on River Deltas

9:30 **Siddarth Misra,** University of Oklahoma
Non-Invasive Static Fracture Characterization Based on
Data-Driven Analysis of Ultrasonic Measurements

10:00 **Bill Carey/Hari Viswanathan,** Los Alamos National Laboratory
Fracture Flow Emerging from Coalescence, Branching,and Network Geometry

10:30 Break

Session VI, Chair: Paul Fenter, ANL

10:45 **Jose Martinez-Lorenzo,** Northeastern University
Sensing and Imaging Porous Media at Speed using
Information-Theory in 4D and Fused Thermoacoustic, Electromagnetic, and
Acoustic/Seismic Wavefields

11:15 **Tony Ladd,** University of Florida
Dissolution at the Pore Scale: Comparing Simulations and Experiments

11:45 **Ruben Juanes,** MIT
Impact of Wettability on Multiphase Flow and Granular Mechanics:
Experiments, Modeling, and Theory

12:15 Working Lunch

Wednesday Afternoon

Session VII, Chair: Pupa Gilbert, U Wisconsin

1:30 **Charlie Werth**, U Texas Austin
Mineral Alteration of Shales by CO2 and Brine Containing Surfactants

2:00 **Louise Criscenti**, Sandia National Lab
Interfacial Geochemistry of Nanopores: Molecular Behavior in Subsurface Environments

2:30 **Andrew Stack**, Oak Ridge National Lab
Effect of an Impurity on Nucleation and Growth of Barite; Implications for Porosity and Permeability Evolution in Porous Media

3:00 Break

Session VIII, Chair: Sue Brantley, Penn State

3:15 **Alexis Navarre-Sitchler**, Colorado School of Mines
Experimental Determination of Mineral Dissolution Rates at the Pore Scale Using Microfluidic Approaches

3:45 **Ian Bourg**, Princeton
Mineral-Organic Interactions in Soils and Sediments

4:15 **David Cole**, Ohio State
Nanopore Confinement of C-H-O Mixed-Volatile Fluids Relevant to Subsurface Energy Systems

4:45 Break

5:00 **Laura Lammers**, Lawrence Berkeley National Lab
Progress one Understanding Structure-Composition Feedbacks in Clay-Rich Materials

-Dinner on your own-

Wednesday Evening

7:30 **David Yuen**, Columbia
Applications of Machine Learning and Deep Learning to Crustal Geodynamical Problems

8:15 **Poster Session II**

Thursday Morning

7:00 Breakfast

Session IX, Chair: Laura Pyrak-Nolte, Purdue

8:00 **Yehuda Ben-Zion**, University of Southern California
Properties and Dynamics of the Shallow Crust

8:30 **Wenlu Zhu**, University of Maryland
Effect of Pore Fluid Pressure on Slip Instability Beyond Effective Stress Threshold

9:00 **Emily Brodsky**, UC Santa Cruz
Induced Seismicity in a Faulty Crust

9:30 Break

Session X, Chair: Arndt Schimmelmann, Indiana U

9:45 **John Eiler**, Caltech
Foundations of Molecular Isotomics

10:15 **Abby Kavner**, UCLA
Electrochemical Kinetics of Stable Isotopes

10:45 **Aradhna Tripati**, UCLA
Progress on Fundamentals and Frontiers in Carbonate Clumped Isotope Geochemistry

Posters

Kevin Rosso, PNNL	"Unravelling the Structure and Phase Transformation Pathways of Ferrihydrite"
Piotr Zarzycki, LBNL	"Dielectric Properties of the Electrical Double Layer at the Mineral/Electrolyte Interface"
Trish Dove, VA Tech	"Metastable Solubility and Local Structure of Amorphous Calcium Carbonate"
Bill Casey, UC Davis	"Expanding NMR Capabilities with Optical Detection"
Jacky Bracco, CUNY	"Cation Sorption at the Barite (001)-Water Interface"
Neil Sturchio, Delaware	"Flow Rate and Ionic Strength Effects on Calcite Reactivity in Microchannels"
Sebastien Kerisit, PNNL	"Molecular-Scale Controls on Heterogeneous Nucleation and Growth of Carbonates at Mineral/Water Interfaces"
Arndt Schimmelmann, Indiana	"Genesis, Storage, and Leakage of Shale Gas"
Sue Brantley, Penn State	"Investigating Roughness and Advance Rate of the Weathering Interface in Shale: From Geochemistry to Geophysics"
Hsiu-Wen Wang, ORNL	"Ion Association in Concentrated Aqueous Salt Solutions: Concentration-Dependent Reaction Dynamics"
Stephan Irle, ORNL	"Density-Functional Tight-Binding for Geochemical Simulations: Recent Progress in Method Development and Geochemical Applications"
Robert Eagle, UCLA	"Combining geochemical tracers and cellular biological approaches to study the biomineralizing environment of marine calcifying organisms"
Pupa Gilbert, Wisconsin	"Biomineralization by Particle Attachment in Early Animals"
Anastasia Ilgen, SNL	"Adsorption and Coordination Environment of Cations under Nano-Scale Confinement"
Adam Wallace, Delaware	"Forward Flux Sampling Simulations of Water Exchange Reactions on Pico- to Micro-Second Timescales"

Properties and Dynamics of the Shallow Crust

Yehuda Ben-Zion
Department of Earth Sciences, University of Southern California, Los Angeles, CA, 90089-0740, USA

Abstract

I review multi-scale/signal seismological results on imaging the top few hundred meters of the crust, monitoring temporal changes of seismic velocities, and efforts to detect and classify different sources of weak ground motion contained in continuous seismic waveforms. The studies utilize data recorded by dense seismic arrays and borehole sensors. The results indicate that the sub-surface material has extreme seismic properties (very low Vp, Vs, Q values; very high Vp/Vs ratios) that make it is highly susceptible to failure and temporal changes. Large earthquakes produce rock damage (reduction of Vp, Vs, Q) in broad shallow regions around the rupture zones. The co-seismic changes in the top 100 m or so are very large (>30-50% velocity reduction) and are followed by log(t) recovery. Continuous seismic waveforms consist mostly of motion generated by wind-related shaking of obstacles above the ground, aircraft/train/truck/car signals, and other natural & anthropogenic sources producing earthquake- and tremor-like signals. We are in the process of using different types of sources of weak ground motion (genuine small earthquakes, wind, air-traffic, trains etc.) to train machine learning algorithms for efficient detection of these sources.

Mineral-organic interactions in soils and sediments

Ian C. Bourg

Civil and Environmental Engineering & Princeton Environmental Institute, Princeton University, Princeton NJ 08544, USA (bourg@princeton.edu)

Soil carbon is the largest pool of carbon near the Earth's surface, about as large as the atmosphere, biosphere, and surface ocean combined. This soil carbon pool has important implications for the Earth's carbon budget. For example, soils presently act as a net carbon sink that absorbs ~ 2 Gt_C per year ($2/10^{ths}$ of anthropogenic CO_2 emissions). This carbon sink is sensitive to changes in temperature, rainfall, and soil management techniques, but a detailed predictive understanding of its magnitude remains elusive. One clue into the fundamental basis of this carbon sink is that soil carbon content correlates most strongly with the content of the finest-grained soil minerals (particularly smectite clay minerals in temperate soils and Fe and Al oxides in soils exposed to intense weathering).

Here, we present molecular dynamics (MD) simulations that aim to gain insight into one possible fundamental control on the so-called "mineral protection" of soil carbon: the adsorption of organic molecules on clay mineral surfaces. In particular, we describe our recent development and validation of an MD simulation methodology that predicts the affinity of organic molecules for smectite clay surfaces. Specifically, we present results on the adsorption of ten different organic molecules with a range of molecular weights and hydrophilicities (phthalate esters, polycyclic aromatic hydrocarbons, and perfluorinated alkyl substances) on a stack of smectite clay nanoparticles. Our results show that organic molecules consistently have a strong affinity for the clay surfaces. Contrary to prominent theories of soil carbon mineral protection, this affinity is primarily entropic in nature. In short, the tendency of soil carbon to become associated with mineral surfaces is determined primarily by hydrophobic interactions rather than by the interaction of specific organic functional groups with the mineral surface.

Cation Sorption at the Barite (001) – Water Interface

Jacquelyn N. Bracco[1*], Sang Soo Lee[1], Joanne E. Stubbs[2], Peter J. Eng[2,3], Paul Fenter[1], James D. Kubicki[4], and Andrew G. Stack[5]

[1] Chemical Sciences and Engineering Division, Argonne National Laboratory, Argonne, IL
[2] Center for Advanced Radiation Sources, University of Chicago, Chicago, IL
[3] James Franck Institute, University of Chicago, Chicago, IL
[4] Geological Sciences, University of Texas- El Paso, El Paso, TX
[5]Chemical Sciences Division, Oak Ridge National Laboratory, Oak Ridge, TN
[*]Current address: School of Earth and Environmental Sciences, Queens College, City University of New York, Flushing, NY

Ionically-bonded minerals are ubiquitous and play a determinative role in controlling the mobility of toxic metals in natural environments. To understand this controlling mechanism, here we use barite as a model substrate to examine how sparingly soluble minerals interact with toxic metals using a combination of experimental and theoretical methods. High resolution X-ray reflectivity (XR) and resonant anomalous X-ray reflectivity (RAXR), were used to quantify structural changes at the barite (001) – water interfaces arising from Sr^{2+} and Pb^{2+} sorption. The XR results in the absence of added Sr^{2+} or Pb^{2+} identified four distinct adsorbed species. Comparing these results with classical molecular dynamics (CMD) simulations reveals that these species are adsorbed water molecules, each of which coordinates one or two surface ions (either barium, sulfate, or both). These water molecules also adsorb in lateral positions consistent with those of bariums and sulfates in the bulk crystal lattice. The XR results in the presence of added Sr^{2+} or Pb^{2+} indicate that these ions disrupt the surfaces of barite to a greater extent than in the absence, with Pb^{2+} disrupting the surfaces more than Sr^{2+}. Density functional theory (DFT) calculations predict that Sr^{2+} substitutes for barium ions in the top layer of the barite surface as well as adsorbs onto the surface (Figure 1). Comparisons between RAXR measurements, DFT, and CMD simulations reveal this adsorbed Sr^{2+} binds to the oxygens on sulfate molecules. The RAXR results at the barite – Pb-rich solution interface show that Pb^{2+} also incorporates and adsorbs to the barite (001) surface. Pb^{2+} sorbs at $[Pb^{2+}] \geq 6$ μM, above which the coverage increases with increasing $[Pb^{2+}]$. This sorption behavior of Pb^{2+} can be described using a classical Langmuir isotherm. In contrast, Sr^{2+} sorption is only significant at $[Sr^{2+}] \geq 25$ μM, upon which the coverage increases rapidly before the coverage saturated. This unusual sorption behavior of Sr^{2+} can be described using a Frumkin isotherm. Bond valence theory was used to confirm that barite (001) in the absence of foreign ions is neutral to slightly positively charged in circumneutral pH conditions. This suggests that cation adsorption is not initially driven by electrostatic attraction. Together, these experimental and theoretical results demonstrate simple single-site adsorption models may be less useful for describing sorption behavior at the surfaces of ionically-bonded minerals than covalently-bonded minerals, due to varying extents of incorporation for different cations at the sparingly-soluble mineral surfaces.

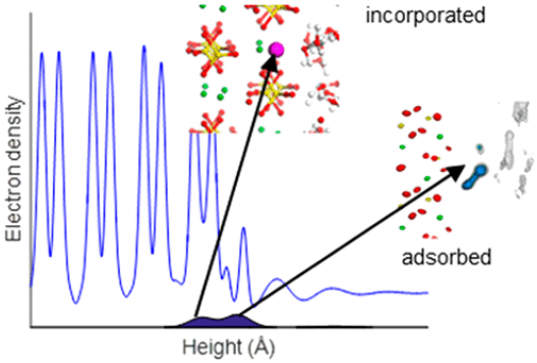

Figure 1. Adsorption and Incorporation of Sr^{2+} revealed by a combination of experimental and theoretical techniques.

Bracco, J. N.; Lee, S. S.; Stubbs, J. E.; Eng, P. E.; Heberling, F.; Fenter, P.; Stack, A. G. *The Journal of Physical Chemistry C* **2017** *121* (22), 12236-12248. DOI: 10.1021/acs.jpcc.7b02943

Bracco, J. N.; Lee, S. S.; Stubbs, J. E.; Eng, P. E.; Jindra, S.; Warren, D. M.; Kommu, A.; Fenter, P.; Kubicki, J. D.; Stack, A. G. *The Journal of Physical Chemistry C* **2019** *123* (2), 1194-1207. DOI: 10.1021/acs.jpcc.8b08848

Induced Seismicity in a Faulty Crust

Emily E. Brodsky, UC Santa Cruz

Human-induced seismicity poses both a societal challenge for subsurface energy production and an intellectual challenge for our understanding of the fundamental processes governing rock failure. Meeting these challenges requires ways to measure and compare induced seismicity at sites across the globe. In our initial project, we found that the spatial distribution of earthquakes is a powerful tool for the evaluation of failure mechanisms and induced stress changes. Unusually distant earthquakes in Oklahoma led to an appreciation of the effects of large injection fields in poroelastic media. A comparison of spatial distributions globally led to the discovery that injection into sedimentary rocks can produce larger, more distant earthquakes than comparable injection into basement. Each of these induced earthquakes has the potential to trigger more earthquakes by interacting with the local faults. We have examined fault interaction by studying the aftershock productivity of induced seismicity compared to ordinary, tectonic earthquakes. We find that induced seismicity in Oklahoma usually produces aftershocks at a similar rate to California, with the notable exception of during mitigation efforts. When wells are shut-in immediately after mainshocks, aftershock productivity drops even at large distances from the wells. The observations suggest that the high aftershock productivity in Oklahoma is a result of system-wide fault activation as might be expected due to poroelastic stresses rather than channelized fluids activating individual faults.

Compaction localization analyses based on a Breakage Mechanics theory for anisotropic granular solids

G. Buscarnera[1], F. Marinelli[2], and G. Shahin[1]
[1]*Northwestern University*
[2]*Plaxis bv, formerly Northwestern University*

All granular materials display to a certain extent anisotropic properties which influence frictional strength and volume change. In case of geophysical solids, such directional dependence is affected by their deposition history, which generates spatially-varying networks of grain contacts, damage zones and bedding planes. Taking into account such effects at the continuum scale has traditionally been a formidable challenge. For example, most constitutive laws for anisotropic geomaterials introduce an intrinsic reference frame through tensorial expressions which rotate and distort the yield surface. This strategy, although effective, requires a non-trivial mathematical representation of the orientation-dependent characteristics of the rock and difficult calibration procedures. In this project, we are developing a Breakage Mechanics theory aimed at disclosing the link between strain energy storage and the yield surface of granular rocks. The thermodynamic structure of our framework enables us to express the energy release resulting from comminution as a function of an elastic energy potential. As a result, the model captures without additional fitting parameters the dependence of the yield envelope on the orientation of bedding planes and loading direction. The performance of the model has been tested against laboratory tests available for two sandstones. Despite its simplicity, the new model discloses an intimate connection between grain-scale strain energy release and cataclastic yielding, thus considerably simplifying the description of inelastic anisotropy. Such findings also enrich the ability of the Breakage Mechanics framework formulated in the previous stages of the project, in that they enable the simulation of creep in fluid-saturated anisotropic rocks, as well as the study of strain localization patterns with concurrent comminution.

The current project activities are focused on the connection of multi-scale constitutive models with laboratory tests assisted by X-ray microtomography. For this purpose, a procedure to initialize the variables of a constitutive law on the basis of digital images has been developed. The approach was tested against experiments conducted on the Tuffeau de Maastricht, a high-porosity carbonate rock displaying compaction localization across a wide range of confinement pressures. Porosity maps extracted from digital images were used to define a numerical replica of the sample which allowed the initialization of the model parameters at each Gauss point of a finite element mesh. The model was able to capture accurately the evolution of the reaction force exerted by the sample after the yielding point, thus capturing the re-hardening stage emerging after the achievement of a threshold porosity. In addition, the model replicated the propagation of a compaction front from the boundaries up to the point of re-hardening. Future analyses will focus on the inspection of heterogeneous compaction zones developing during creep and/or relaxation tests in fluid-saturated specimens, and will test the proposed constitutive theories in light of data generated with a new testing device specifically designed to track the concurrent evolution of porosity and grain size distribution in granular materials.

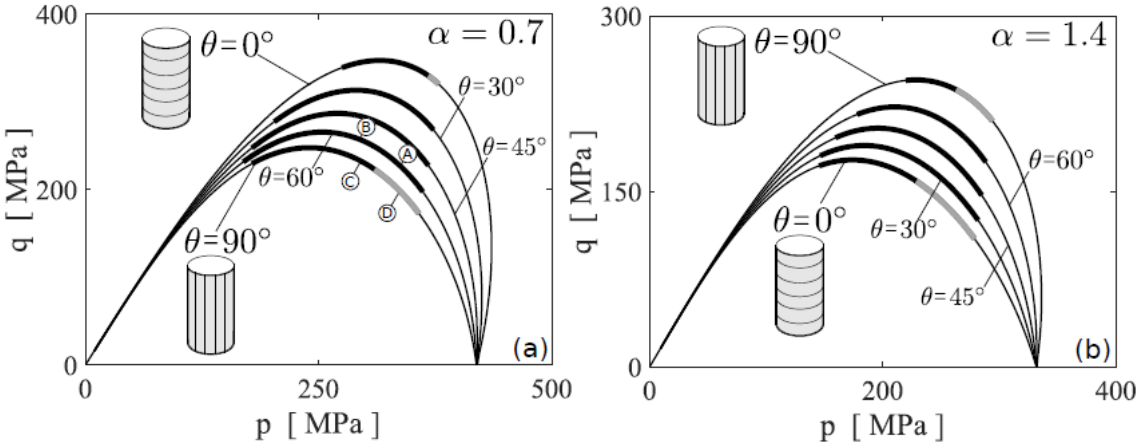

Figure 1. Predicted alteration of the yield surface of a granular rock for varying bedding plane inclination, θ, and elastic anisotropy coefficient, α (α >1 indicates a stiffer response parallel to the bedding planes, while α <1 indicates the opposite case). Isotropic linear elasticity is recovered for α =1. The model captures changes in the size and location of the compaction localization domain due to changes in relative orientation between loading directions and intrinsic material reference system (thick solid lines sketched on top of the predicted yield surfaces).

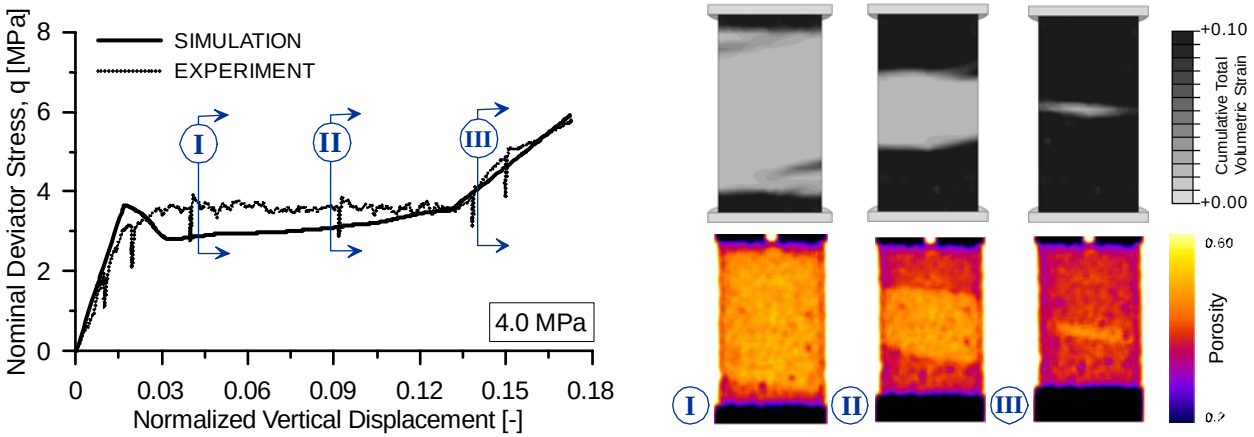

Figure 2. Example of simulated deformation response of Tuffeau de Maastricht subjected to triaxial compression. The analysis is based on a constitutive law initialized with porosity measurements obtained from X-Ray microtomography, as well as on values of boundary friction compatible with those reported for the adopted testing apparatus. The results show a satisfactory ability of the model to replicate the spatial patterns of compaction propagation.

Recent Publications

Marinelli, F., Buscarnera, G. (2019). Anisotropic Breakage Mechanics: from stored energy to yielding in transversely isotropic granular rocks. *Journal of the Mechanics and Physics of Solids*, 129, 1-18.

Shahin, G., Papazoglou, T., Marinelli, F., Buscarnera, G. (2019). Simulation of localized compaction in Tuffeau de Maastricht based on evidence from X-ray tomography. To appear in *International Journal of Rock Mechanics and Mining Sciences*.

Shahin, G., Marinelli, F., Buscarnera, G. (2019). Viscoplastic interpretation of localized compaction creep in porous rock. To appear in *Journal of Geophysical Research – Solid Earth*.

Sohn, C., Buscarnera, G. (2019). Measurement and simulation of comminution rate in granular materials subjected to creep tests. To appear in *Granular Matter*.

Fracture Flow Emerging from Coalescence, Branching and Network Geometry

J. William Carey and Hari S. Viswanathan

Natural and induced fractures act as fluid conduits enabling orders of magnitude faster flow than through the adjacent rock matrix. As a consequence, predicting and controlling fracture permeability is critical to many subsurface energy applications. Observations in nature and the laboratory consistently show that fractures are often rough, branched, and segmented structures that interact to form complex, intersecting networks. Such structures are far from the simple-planar features that have been used to establish fundamental understanding of fracture behavior including friction, permeability, displacement, and self-healing. Recognizing this complexity, our study involves direct experimental observations of fracture formation and fluid flow at subsurface conditions coupled with high-fidelity numerical simulations of complex fracture networks. In this presentation, we describe experimental studies of fracture permeability and anisotropy obtained by triaxial direct-shear methods coupled with x-ray radiography and tomography in the context of developments of our en échelon theory. We investigate subsequent modifications to fracture permeability induced by reactive flow in shale and cement using both triaxial direct-shear and microfluidics methods. In both experiments and models, we characterize fracture network permeability in terms of percolation theory. We are currently developing theory and have numerical results that explain fracture branching processes during hydraulic fracturing and have preliminary experiments illustrating our approach.

Optically Detected NMR on Aqueous Geochemical Solutions

Dylan Sures, Zhipan Wang, Louis Steele, Nicholas Curro, and **William H. Casey**

Isotope-substitution reactions are particularly useful for understanding pathways for aqueous reactions and Nuclear Magnetic Resonance (NMR) methods are a standard tool because it samples molecular dynamics at timescales ranging from nanoseconds to hours. In the last funding period we perfected an NMR probe based upon piston-cylinder technology and used it to establish reactivity trends at GPa pressures. The instrument uncovered surprising new results about the fundamental properties of solutions, including enhanced colligative properties, direct measurements of changes in speciation and changes in solute transport at GPa pressures.

This technology is, however, limited to pressures less than only a couple of GPa because NMR signals are conventionally detected by the current induced in a Faraday coil surrounds that the sample, with the entire apparatus placed in a superconducting magnet to induce a large $\mathbf{B_o}$ field. In a standard experiment, $\sim 10^{20}$ spins are polarized and the signal both induced and detected via an adjacent coil, which must surround a volume of dozens of microliters to milliliters. The low sensitivity of NMR detection via these induction coils limits high-pressure solution NMR to a few GPa if the goal is to detect solutes. Of, course, NMR has been adapted to diamond-anvil cells (DAC), but these studies are almost invariably on bulk materials (e.g., water, alcohol), not solutes in water (e.g., $AlO_4Al_{12}(OH)_{24}(OH_2)_{12}^{7+}(aq)$).

New quantum-sensing technology can extend the capabilities enormously if the Faraday induction coil is replaced with optical detection of magnetism. NMR spectra could be collected with light from nanoliters or less of solution on top of fluorescing defect centers in diamonds (Figure). Electrons in the defect center are exquisitely sensitive to adjacent magnetic fields and release light as a function of spin state. This detector will fundamentally transform NMR spectroscopy on geological materials because:

- **(i)** sample volumes are reduced to submicroliters and sometimes subnanoliters. Diamond-anvil cells (DAC) can be employed as reactor vessels;
- **(ii)** the sensing technology is inherently an interfacial method;
- **(iii)** NMR spectroscopy is freed from expensive cryogenic cooling and large magnets;
- **(iv)** an NMR spectrometer decreases in size from a room to a table-top instrument;
- **(v)** magnetic fields can be imaged at micrometer scales or less.
- **(v)** sensing could be via diamond nanoparticles dispersed in the fluid.

This research expands the ***type*** of research accessible to aqueous geochemists and aligns with the goal of DOE/OBES: *'To control and manipulate matter at the level of atoms and electrons.'*.

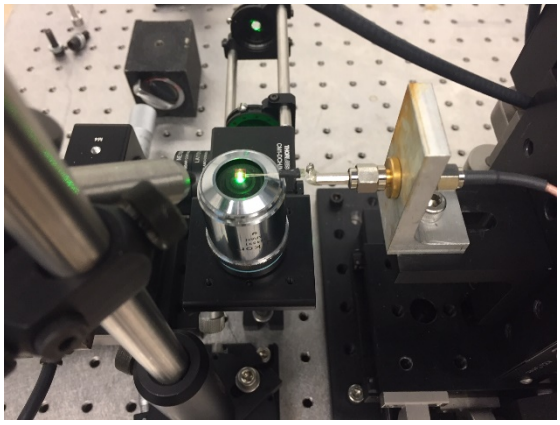

Figure (left): An NMR spectrometer for subnanoliter volumes can be constructed using optical detection. A left, a diamond is excited by green light (532 nm) and fluorescing red light, with a microwave antenna to excite the electrons. The column is a standard microscope objective.

Nanopore Confinement of C-H-O Mixed-Volatile Fluids Relevant to Subsurface Energy Systems

David R. Cole, PI; Philip Grandinetti, Co-PI
The Ohio State University, Columbus, OH 43210

Collaborating Scientists:
Alberto Striolo, University College London
Gernot Rother, Oak Ridge National Laboratory
Eugene Mamontov, Oak Ridge National Laboratory

Although our understanding of the full range of pore features developed in various geological settings continues to advance, we expect that the thermo-physical behavior of complex supercritical C-O-H fluids in nano-confined geometries will exhibit significant differences compared to bulk fluids. There is general agreement that the collective structure and properties of bulk fluids such a CH_4, C_2H_6 and CO_2 are altered by solid substrates, confinement between two mineral surfaces or in narrow pores due to the interplay of the intrinsic length scales of the fluid and the length scale of confinement. The resulting interfacial areas (fluid-fluid, and mineral-fluid) are relatively large within the pore volume and therefore control chemical and transport behavior in shale and other earth materials containing nanopore regimes. The combined effect of intermolecular forces that vary among different mineral systems and fluid confinement results in unique (and, poorly constrained) perturbations to a wide range set of thermodynamic and transport parameters, different from those observed in the bulk phase. It is a formidable challenge to characterize the fluid behavior (e.g. phase transitions, molecular orientation and relaxation, diffusion, adsorption, contact angle, surface tension, etc.) within internal nano-pore or fracture networks. *The overarching goal of this effort is to develop a fundamental, molecular- to macroscopic-level understanding of the sorptivity, structure, dynamics and reactivity of C-O-H fluids at mineral surfaces or within nanoporous matrices for temperatures, pressures and compositions encountered in energy-relevant near-surface and shallow crustal environments.*

This presentation will provide an overview of the application of state-of-the-art experimental, analytical and computational tools to assess key features of the fluid-matrix interaction. The multidisciplinary approaches highlighted will include neutron scattering, thermodynamic measurements and molecular-level simulations to quantitatively assess molecular properties of different mixtures of C-O-H fluids in nanpores. Examples of key results include:

- The tortuosity of the pore network (e.g., ZSM-5 silica) has a profound impact on hydrocarbon mobility – i.e., fast in straight pores, faster yet at pore channel intersections, but much slower in sinusoidal channels and at pore entrances.
- The mobility of a hydrocarbon (methane, propane, butane) is enhanced in the presence of another non-polar fluid such as CO_2 due to the preference for CO_2 to adsorb and wet SiO_2 pore walls.
- The methane solubility in water is enhanced in silica nanopores at elevated pressures and ambient temperature compared to bulk values.
- The methane solubility in nano-confined water strongly depends on the confining substrate – SiO_2>$Al_2O_>$ >MgO due to a more disordered water density distribution on SiO_2 (i.e., less hydrophilic).
- The diffusivity of methane in nanopores is highly dependent on substrate type and its effect on water structure, its free energy landscape and hydrogen bonding on the surface where the order for methane diffusion rate is SiO_2>MgO>Al_2O_3>muscovite≅calcite.
- The preferential adsorption of either CO_2 or H_2O on the pore surface can affect the equilibrium conversion of CO_2 to CH_4, i.e., $CO_2 + 4H_2 = CH_4 + H_2O$

Interfacial Geochemistry of Nanopores: Molecular Behavior in Subsurface Environments

Louise J. Criscenti, Anastasia G. Ilgen, Jeffery A. Greathouse, and Kevin Leung
Geochemistry Department, Sandia National Laboratories

The two main themes of our project are to investigate the impact of nanoconfinement on interfacial chemistry between geomaterials and aqueous solutions and how nanoscale confinement is reflected at the mesoscale. To examine the role of confinement, we conduct batch adsorption experiments on synthetic mesoporous silica and alumina with controlled pore sizes; and, for comparison, on non-porous amorphous silica and alumina. X-ray absorption spectroscopy (XAFS) is used to compare the types of adsorption complexes that form on non-porous and materials with 2-nm, 4-nm, or 8-nm pores. In addition, *ab initio* molecular dynamics (AIMD) potential of mean force (PMF) calculations are performed to establish the relative energetics of cation adsorption on an unconfined surface, and classical molecular dynamics (CMD) is used to look at the effects of nanoconfinement. For Cu(II) adsorption to porous silica, our results suggest that Cu(II) adsorbs as an inner-sphere complex, readily forms $CuOH^+$ complexes in solution, and forms polymeric complexes under nanoconfinement.

To link nanoscale confinement to mesoscale phenomena, we investigated the diffusion of water from a large pore into the interlayer of a Na-montmorillonite particle using CMD. This effort required the use of new ClayFF parameters for clay edges (Pouvreau et al., 2019), and the modification of Lennard-Jones interaction parameters for interlayer Na^+ with the bridging oxygen atoms of the siloxane surfaces. PMF calculations were performed to determine both the relative energetics of Na-montmorillonite with no interlayer water (0W), one water layer (1W), and two water layers (2W); and to calculate possible transition states between these three hydration states. The simulations suggest that hydrogen-bonding between layer edge groups make an important contribution to the energy barrier for initial hydration.

Papers published in 2018 and 2019

Criscenti, Ho, and Hart (2018) Structural Properties of Aqueous Solutions at the (100) and (101) Goethite Surfaces by Molecular Dynamics Simulation. *Langmuir* 34, 14498-14510.

Harvey, Johnston, Criscenti, and Greathouse (2019) Distinguishing Between Bulk and Edge Hydroxyl Vibrational Properties of 2:1 Phyllosilicates via Deuteration. C*hemical Communications* 55, 3453-3456. [Inside Back Cover]

Ho, Criscenti, and Greathouse (2019) Revealing Transition States during the Hydration of Clay Minerals. *Journal of Physical Chemistry Letters*, 10, 3704-3709.

Ho, Greathouse, Lee, and Criscenti (2018) Enhanced Ion Adsorption on Mineral Nanoparticles. *Langmuir* 34, 5926-5934.

Ilgen, Kukkadapu, Leung, and Washington (2019) Switching on Iron in Clay Minerals. *Environmental Science Nano*. DOI: 10.1039/c9en00228f. [Back Cover]

Knight, Kalugin, Coker, and Ilgen (2019) Water under Nano-scale Confinement. *Scientific Reports* 9, 8246.

Leung, Criscenti, Knight, Ilgen, Ho, and Greathouse (2018) Concerted Metal Cation Desorption and Proton Transfer on Deprotonated Silica Surfaces. *Journal Physical Chemistry Letters* 9, 5379-5385.

Pouvreau, Greathouse, Cygan, and Kalinichev (2019) Structure of Hydrated Kaolinite Edge Surfaces: DFT Results and Further Development of the ClayFF Classical Force Field with Metal-O-H Angle Bending Terms. Submitted to *Journal of Physical Chemistry C* 123, 11628. DOI: 10.1021/acs.jpcc.9b00514.

Acknowledgements

This material is based upon work supported by the U.S. Department of Energy, Office of Basic Energy Sciences, Division of Chemical Sciences, Geosciences, and Biosciences. Sandia National Laboratories is a multimission laboratory managed and operated by National Technology and Engineering Solutions of Sandia, LLC., a wholly owned subsidiary of Honeywell International, Inc., for the U.S. Department of Energy's National Nuclear Security Administration under contract DE-NA-0003525. This paper describes objective technical results and analysis. Any subjective views or opinions that might be expressed in the paper do not necessarily represent the views of the U.S. Department of Energy or the United States Government.

Modern computational chemistry methods on advanced computer architectures are now capable of predicting the properties of a broad range of systems including their reactivity with enough reliability to provide useful information for geochemical applications. The talk will describe benchmarking lower level electronic structure methods against coupled cluster CCSD(T) theory. Examples of combining explicit/implicit solvent models will also be described. Applications include metal carbonates and bicarbonates as well hydrated forms, nanoparticle growth to the bulk, the pK_a's of metal ions, the energetics of CO_2^-, and the formation of Brönsted acids from Lewis acids and water. This work is supported by the U.S. DOE Office of Science, Basic Energy Sciences.

METASTABLE SOLUBILITY AND LOCAL STRUCTURE OF AMORPHOUS CALCIUM CARBONATE (ACC)

Sebastian T. Mergelsberg,[1]* James J. De Yoreo,[2] F. Marc Michel,[1] J. Donald Rimstidt,[1]† and Patricia M. Dove[1]*

[1]Department of Geosciences, Virginia Tech, Blacksburg, VA 24061, USA
[2]Physical Sciences Division, Pacific Northwest National Laboratory, Richland, WA 99354, USA.
[3]Department of Materials Science and Engineering, University of Washington, Seattle, WA 98195, USA.
† Deceased.
* Corresponding author. Email: sebastian.mergelsberg@pnnl.gov

Calcium carbonate minerals are an essential component in many invertebrates, with good examples found in the exoskeletons of sea urchins, mollusks, and crustaceans. Many of these animals have produced polymorphs of $CaCO_3$ as biominerals over long periods of geologic time, thus recording composition patterns (Mergelsberg et al., 2019) in the evolution of organisms, as well as isotopic information about their environment and biological processes. The formation of minerals that comprise these skeletal structures often begins by precipitating an amorphous intermediate phase, such as amorphous calcium carbonate (ACC) but little is known about reactive pathways involving these materials (De Yoreo et al., 2015). Thus, an understanding of ACC properties — both chemical and physical — is critical to establishing the crystal growth processes and the consequent signatures that are recorded during $CaCO_3$ biomineralization.

The properties of amorphous calcium carbonate (ACC) provide the foundation for understanding the mineralization of calcified skeletons. However, studies of ACC structure and composition present inconsistencies that suggest the physical picture is incomplete. To test the idea that the chemical and structural properties of ACC are regulated by a systematic relationship to the environment of formation, this DOE-BES funded investigation quantifies the metastable solubility and structure of ACC produced under a series of chemical conditions.

Using complementary *in situ* methods that quantify ACC structure (*in situ* PDF analysis) in parallel with chemical composition (TGA, ICP-OES), we find two short-range structures are produced that also show distinct morphological differences (Mergelsberg, et al., *GCA*, in revision). Conditions with high carbonate ion concentrations stabilize a hydrous Ca-rich ACC with a short-range order that is independent of Mg content. In contrast, low carbonate solutions favor anhydrous Mg-rich ACC with mixed Ca- and Mg-short range order. Most conditions produce a physical mixture of both ACC types.

Measurements of solubility product determined from both supersaturated and undersaturated conditions find the distinctive structures are related to solution carbonate activity while apparent solubility is primarily determined by the magnesium content of the solid. Bulk apparent solubility is a composite that concurs with established values. The findings demonstrate the type of ACC that forms is tuned by Mg^{2+} and CO_3^{2-} concentrations and suggest ACC structure, not bulk composition, is a reliable indicator of intermediate phase. Evolution between these two types of ACC can be tuned by an interplay of solution CO_3/Ca and Mg activities.

The quantitative connections between ACC structure, chemical environment, and stability presented in this study (Mergelsberg, et al., *GCA*, in revision) provide a basis for interpreting apparent differences between observations of ACC in synthetic and natural systems and invite a better understanding $CaCO_3$ biomineralization processes. Studies of calcification in diverse phyla show sites of mineralization can contain stable hydrated and/or anhydrous forms of ACC (Addadi et al., 2003; Radha et al., 2010; Gong et al., 2012; Mass et al., 2017; Politi et al., 2006). Within these systems, the carbonate anhydrase enzyme is recognized as a ubiquitous molecule that catalyzes both the formation and decomposition of bicarbonate at a wide range of pH values. It is plausible this molecule also regulates local carbonate ion concentration during calcification (Weiner and Dove, 2003) to optimize the type(s) of ACC that forms. For example, anhydrous Mg-ACC should be energetically costly, if not impossible, to precipitate with its slower kinetics. However, by taking advantage of the fast kinetics associated with hydrous Ca-ACC, the transition to the higher solubility anhydrous form can subsequently occur by modulating local carbonate concentration.

Combining geochemical tracers and cellular biological approaches to study the biomineralizing environment of marine calcifying organisms

Authors: Robert Eagle, Maxence Guillermic, Yi-Wei Liu, Robert Ulrich, Ilian De Corte, Jill Sutton, Louise Cameron, Dirk de Beer, Sambuddha Misra, Aradhna Tripati, Justin Ries

Biomineralization in marine calcifying organisms show a wide range of sensitivities to changing temperature and saturation state. This diversity in responses between species is likely the result of complex interplay of factors but two endmember hypotheses highlight a role of the fundamental mechanisms of biomineralization. Firstly, physicochemical hypotheses assume that it is the carbonate chemistry at the site of calcification the primary control over rates of calcification differential ability of organisms to control this chemistry that responsible for varying calcification responses to oceanic change. A second view is that marine calcification is such a highly regulated process involving factors such as amorphous calcium carbonate precursors and organic templating that the process of calcification is relatively insulated from changing external and internal carbonate chemistry, therefore other explanations for diverse calcification responses are more likely. Both models are not necessarily mutually exclusive, put place different emphasis of the relative importance of biomineralization processes in sensitivity to the environment. Here I present the results of a series of experiments that shed addition light on this problem. Firstly, we have revisited archived carbonate material from a landmark culturing study that assessed biomineralization changes in response to saturation state, and conducted measurements of the boron isotopic (□11B) composition – a proxy for calcification pH - of 10 species cultured across 4 different saturation states. We find very diverse results with some species showing tight coupling of calcification rate and □11B derived pH at the site of calcification, consistent with the physicochemical model, and the two parameters are decoupled, suggestive that calcification site pH is not a dominant control over calcification rate changes due in response to changes in external carbonate chemistry. Secondly, I will present the results of more detailed studies on stony corals cultured at a range of temperatures and saturation states, utilizing both the geochemical approach but also using pH microprobes to directly determine the pH of fluid pockets inside the calicoblastic epithelium of corals. □11B and microprobe data are correlated, indicating that the precipitation coral aragonite does occur in the elevated pH fluids of the calcioblastic epithelium, but there are differences in sensitivity between approaches that either reflect subtle differences in the time scale of signal recorded or subtle differences in the microenvironment measured. Both techniques reveal a hitherto underappreciated role of temperature and the coral symbiont in the regulation of calcification fluid pH. Archive material from these experiments will allow new constraints on biological regulation calcification fluid pH and carbonate chemistry regulation on other isotope systems, including □18O and “clumped isotope” composition of carbonates.

Foundations of Molecular Isotomics

P.I. John Eiler, California Institute of Technology, Pasadena CA

Most molecules, particularly organics, exist in a large number (generally thousands to millions) of naturally occurring isotopic forms that differ in their numbers and/or atomic sites of rare isotope substitutions. Natural variations in intramolecular isotopic structure arise because isotopic forms of a given molecule generally differ in thermodynamic stability, rates of irreversible reactions (as well as other physical properties), and probabilities of inheriting rare isotopes from precursors. For these reasons, proportions of molecular isotopic forms can be used to reconstruct conditions and mechanisms of molecular formation, storage and destruction, and thus can address diverse problems in the natural and applied sciences. We are engaged in a research program aimed at developing technology, interpretive tools, and proof of concept applications for the use of intramolecular isotopic structures —i.e., clumped and position specific isotopic properties — to address problems in the geosciences, fundamental chemistry of isotopes, and chemical forensics.

Over the course of the last three years we have established that mass spectrometric measurements of molecular and fragment ions, particularly using Fourier Transform Mass Spectrometry (FTMS), enables the generalized study of molecular isotopic structures in a wide range of organic and inorganic compounds. Mass spectrometry provides higher sensitivity, better limits of precision and greater range of use (i.e., more isotopic forms of more molecules) than other technologies that have been adapted to this purpose; with it, nearly any singly and doubly substituted form of nearly any compound in the H-C-N-O-S-Cl chemical 'family' (among others) is potentially observable, and sample sizes required for most measurements we have attempted are on the order of 1 nanomol. The two significant challenges are relating features of the mass spectrum to individual sites of complex molecules, and mastering the various technical hurdles of our new adaptation of FTMS to high precision, high accuracy isotope ratio analysis.

We will present applications of mass spectrometric techniques to questions that can be addressed by site-specific and clumped isotope effects associated with controlled abiological and biological reactions of amino acids. We established that the ~10's of per mil ^{13}C enrichment typical of the amino acid alanine from carbonaceous chondrites reflects a much larger, ~140 ‰, enrichment of the amine carbon site (i.e., the carboxyl and methyl sites are indistinguishable from common terrestrial organic matter). This insight, combined with prior measurements of molecular average ^{13}C contents of meteoritic organics, serves as the basis for a detailed mechanistic interpretation of the formation of alpha-amino acids and associated aldehydes, amines and carboxylic acids in early solar system materials. We will also present initial applications of these technologies to forensically source chemosynthetic vs. biosynthetic compounds in the human food supply.

Future work in this research program will: Expand the technological tool kit to include FT-ICR instrumentation, which enables studies of isotopic structures of peptides, proteins and other large organic molecules; develop a computational toolkit that will let us quickly predict and interpret complex features of molecular isotopic structures in chemical reaction networks; extend applications to amino acids; and explore new applications to geological biomarkers and uses for chemical forensics problems of criminal and national security significance.

Biomineralization by particle attachment in early animals

Pupa U. P. A. Gilbert, Susannah M. Porter, Chang-Yu Sun, Shuhai Xiao, Brandt M. Gibson, Noa Shenkar, Andrew H. Knoll

Crystallization by particle attachment (CPA) of amorphous precursors has been demonstrated in modern biomineralized skeletons across a broad phylogenetic range of animals. Precisely the same precursors, hydrated (ACC-H_2O) and anhydrous calcium carbonate (ACC), have been observed spectromicroscopically in echinoderms, molluscs, cnidarians, phyla drawn from the three major clades of eumetazoans. Scanning electron microscopy (SEM) here also shows evidence of CPA in tunicate chordates. This is surprising, as species in these clades have no common ancestor that formed a mineralized skeleton and appear to have evolved carbonate biomineralization independently millions of years after their late Neoproterozoic divergence. Here we correlate the occurrence of CPA from ACC precursor particles with nanoparticulate fabric and then use the latter to investigate the antiquity of the former. SEM images of early biominerals from Ediacaran and Cambrian shelly fossils show that the earliest animal calcifiers used attachment of ACC particles to form their biominerals. The convergent evolution of biomineral CPA may have been dictated by the same thermodynamics and kinetics as we observe today.

Probing Dynamics of Mineral-Organic Interactions using Real-time, High-temporal Resolution Energetics

Omar R. Harvey, Department of Geological Sciences, Texas Christian University

The study is targeting the systematic collection and analysis of energetics data for facilitating the further development of experimental and model-driven understanding of dynamics of organic-mineral interactions at the sorbent-water interface. Specifically, we are using high-temporal resolution energetics data - obtained from flow adsorption micocalorimetry (FAMC)- to study the evolution of binding/debinding of low molecular weight non-amino and amino carboxylic acids at the sorbent-water interface of Si-, Fe- and Al-oxides. The presentation will cover results from a new developed suite of highly sensitive flow calorimeters and the real-time, energetics-derived binding/debinding dynamics of selected carboxylates to amorphous SiO_2, nano-crystalline boehmite and ferrihydrite. We are able to measure, resolve and quantify the characteristics of reaction steps through FAMC-derived kinetics and energetics. For examples, overall heats of binding ($\Delta_{bind}H$) for organic molecules to amorphous SiO_2 were on the order of 128 to 430 J mol^{-1}; consistent with bonding strength of organic molecules to SiO_2 being about an order of magnitude lower than ion exchange/electrostatic interactions and 2 orders of magnitude lower than ligand exchange. Results also pointed to the binding/debinding of even the simpliest carboxylate (acetate) on the oxides involving a series of 3 or more unique reaction steps varying in energy trajectory (exothermic versus endothermic), magnitude/strength (bonding energy) and duration with molecular structure and environmental condition (e.g. solution pH).

Adsorption and coordination environment of cations under nano-scale confinement

Anastasia G. Ilgen[1], Andrew W. Knight[2], Poorandokht Ilani-Kashkouli[3], Nadine Kabengi[3], Lourdes Loera,[1] Jacob Harvey[1], Jeff Greathouse[1], Louise Criscenti[1], Kevin Leung[1], and Tuan Ho[1]

[1]Geochemistry Department and [2]Storage and Transportation Department, Sandia National Laboratories, Albuquerque, New Mexico 87185
[3] Department of Geosciences, Georgia State University, Atlanta, Georgia 30303

The goal of our project is to develop a molecular-level understanding of how spatial confinement affects kinetics, energetics, and coordination environment at mineral-water interfaces. To examine the role of confinement, we use synthetic mesoporous silicas with 4-nm and 8-nm pore diameters (SBA-15) (Fig. 1), and non-porous amorphous silica. We use cations such as copper (Cu^{2+}) and lanthanide elements neodymium (Nd^{3+}), europium (Eu^{3+}), terbium (Tb^{3+}), thulium (Tm^{3+}) and lutetium (Lu^{3+}) to examine the adsorption reactions as a function of pore size. With increasing atomic number, the ionic radius of lanthanides decreases, while the hydration energies increase. We use these subtle and systematic variations in the hydration energies and ionic sizes to probe the reactivity of silica surfaces confined within nanometer-scale pores.

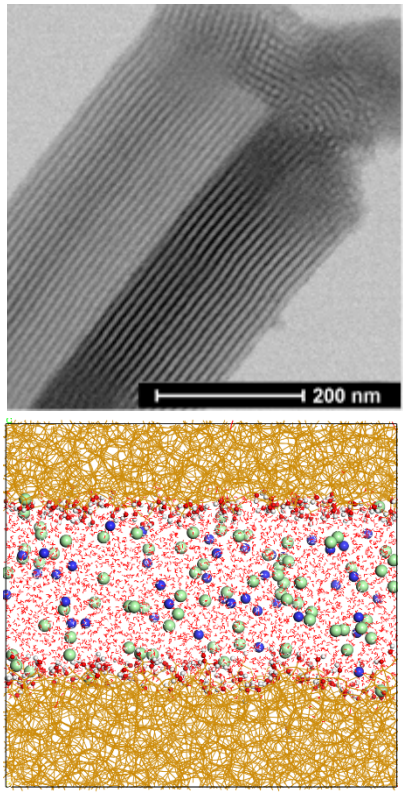

Figure 1. *Transmission electron microscopy image of SBA-15 mesoporous silica (top); Molecular dynamics model of silica pore (bottom).*

To quantify the overall uptake, we determine aqueous composition by inductively coupled plasma mass spectrometry (ICP-MS). The coordination numbers and bond lengths of adsorbed species are quantified using synchrotron-based X-ray absorption fine structure (XAFS) spectroscopy. The energetics of adsorption are quantified using custom-built flow-microcalorimetry. Complementary molecular dynamics (MD) simulations are used to predict surface speciation of adsorbed Cu^{2+} in silica pores as a function of pore size (Fig. 1). Our batch experiments for Cu^{2+} adsorption onto mesoporous silicas showed that the uptake and kinetics of adsorption are enhanced by nano-scale confinement (Knight et al., 2018). Adsorption is pore-size-dependent, and silica with 4-nm pores is more reactive than silica with 8-nm pores. Our analysis of XAFS data indicate that on the surfaces of silica with 4-nm pores, the formation of Cu-Cu poly-nuclear species is promoted (Knight et al., in prep). Our MD simulations further confirm that Cu-Cu polymerization is promoted with increasing degree of spatial confinement (Knight et al., in prep). Microcalorimetry measurements demonstrate that the mechanism of Cu^{2+} adsorption differs for non-porous *versus* porous silicas: adsorption on non-porous silica is an endothermic process, while adsorption within nano-scale pores is exothermic.

In the lanthanide study, we found that whether adsorption onto mesoporous silicas is pore-size dependent is a function of ionic radius and hydration energy (Ilgen et al., in prep). Pore-size dependent adsorption is seen for the lighter (larger) examined elements: Nd^{3+}, Eu^{3+}, and Tb^{3+}, while no such dependence is seen for Tm^{3+} and Lu^{3+}. When pore-size-dependence is observed for lanthanides, silica with 4-nm pores has a higher uptake than silica with 8-nm pores, consistent with our Cu^{2+} results. The

XAFS data supports the batch adsorption studies: Nd^{3+} shows pore-size-dependence in the coordination environment of the 1st Nd-O shell (Fig. 2). No such dependence on pore size is observed for the Lu-O shell for adsorbed Lu^{3+} (Fig. 2). Our XAFS data for non-porous silica, as well as silica with 4-nm and 8-nm pores is shown in Fig. 2.

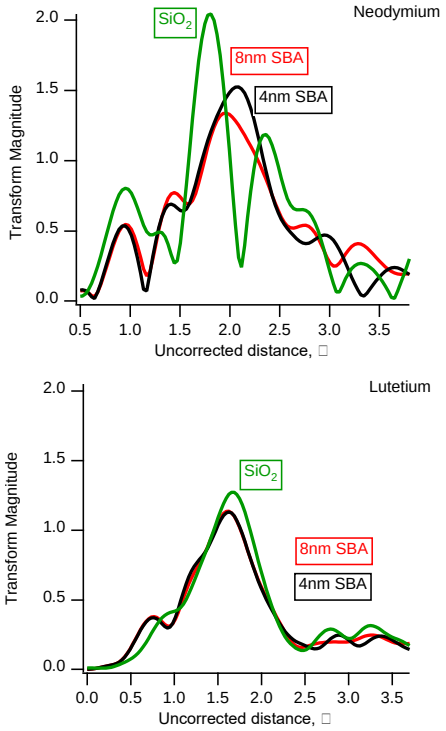

***Figure 2**. X-ray absorption fine structure data for neodymium (top) and lutetium (bottom). Pore-size dependence is observed for neodymium, but not for lutetium.*

Taking the batch and XAFS observations together, we conclude that there is a threshold in the hydration energy, above which no nano-scale confinement effects are observed for silica surfaces confined within 4-nm and 8-nm pores. The lanthanide hydration energy increases (becomes more negative) from -3278 kJ mol^{-1} for Nd^{3+}, to -3556 kJ mol^{-1} for Lu^{3+}. The hydration energy of Cu^{2+} is lower than for lanthanides: -2130 kJ mol^{-1}. The coordination number for lanthanides in water decreases from 9 for Nd^{3+} to 8 for Lu^{3+}. With decreasing hydration number, and increasing (more negative) hydration energies, dehydration reactions become more energetically costly. Therefore, when the hydration energy of a cation is higher than about -3300 kJ mol^{-1}, no nano-scale confinement effects on adsorption are observed for silica surfaces, at least for the surfaces confined inside 4-nm pores. The pore-size effects would likely be seen for smaller pore sizes. We are running complementary micro-calorimetry experiments to quantify the energetics of lanthanide adsorption onto non-porous and porous silica surfaces to characterize reaction pathways.

Papers supported by BES, published in 2018 and 2019

Ilgen A.G., Kukkadapu R.K., Leung K., and Washington R.E. (2019). "Switching on" iron in clay minerals. *Environmental Science Nano.* [Front cover]. DOI: 10.1039/C9EN00228F

Knight A.W., Kalugin N, Coker E., and Ilgen A.G. (2019) Water properties under nano-scale confinement. *Scientific Reports*, accepted.

Blake J.M., Avasarala S., Ali A.-M.S., Spilde M., Lezama-Pacheco J.S., Latta D., Artyushkova K., Ilgen A.G., Cerrato J.M. (2019) Reactivity of As and U co-occurring in Mine Wastes. *Chemical Geology*. DOI: 10.1016/j.chemgeo.2019.05.024

Barker A.J., Douglas T.A., Ilgen A.G., and Trainor T.P. (2019) Lead and antimony from bullet weathering in newly constructed target berms: chemical speciation, mobilization, and remediation strategies. *Science of the Total Environment*, 658, 558. DOI: 10.1016/j.scitotenv.2018.12.188

Knight A.W., Tigges A.B., Ilgen A.G. (2018) Adsorption of Copper on Mesoporous Silica: The Effect of Nano-scale Confinement. *Geochem. Trans.*, 19, 13. DOI: 10.1186/s12932-018-0057-4

Acknowledgements

This material is based upon work supported by the U.S. Department of Energy, Office of Basic Energy Sciences, Division of Chemical Sciences, Geosciences, and Biosciences. Sandia National Laboratories is a multimission laboratory managed and operated by National Technology and Engineering Solutions of Sandia, LLC., a wholly owned subsidiary of Honeywell International, Inc., for the U.S. Department of Energy's National Nuclear Security Administration under contract DE-NA-0003525. P. Lu at Sandia collected the TEM data. This paper describes objective technical results and analysis. Any subjective views or opinions that might be expressed in the paper do not necessarily represent the views of the U.S. Department of Energy or the United States Government.

Incorporation of Metal Impurities in Fe(III) (oxyhydr)oxides

Eugene S. Ilton
Pacific Northwest National Laboratory

Fe (oxyhydr)oxides are ubiquitous and exert a primary control on coupled redox cycles and the transport of minor but critical metals. In this regard, detailed information on the local coordination environment of impurities is necessary to understand host phase properties, biogeochemical cycling of micronutrients, the long-term stability of impurity/host phase associations, waste forms, and tailoring natural Fe oxides for industrial uses. However, despite many decades of work, how impurities are incorporated in $Fe_xO_yH_z$ is not well constrained.

Extended X-ray absorption fine structure spectroscopy (EXAFS) is the method of choice for determining the local coordination environment of impurities in a host phase. Nonetheless, and in particular for seemingly incompatible dopants, a lack of appropriate standard structures and a priori knowledge concerning thermal disorder, coordination numbers, and potential defect associations can render traditional shell by shell fitting unreliable. Here will describe recent results that used ab initio molecular dynamics (AIMD) informed extended X-ray absorption fine structure (EXAFS) spectra to detail the local coordination environment of U(VI) and Zn associated with hematite. AIMD-informed EXAFS was also employed to determine whether U(VI) can be incorporated into goethite that grows by oriented aggregation (OA). As illustrated below, the unprecedented detail uncovered by AIMD-informed EXAFS can dramatically increase our understanding of metal incorporation in Fe oxides as well as other dopant/host phase relationships.

For uranium, complications for interpreteing the EXAFS of incorporated U include charge balance requirements and, in particular for U(VI), preferred symmetry. For example, studies attempting to incorporate U(VI) into hematite by hydrothermal maturation of ferrihydrite (fh) have analyzed nearly identical EXAFS data but with very different interpretations: 1) uranium assumes a uranyl configuration with two short U-O bonds in regular Fe(III) structural sites or 2) roughly equal amounts of uranium assume uranate and uranyl coordination in structural and surface sites, respectively.[1, 2] In contrast to prior studies, AIMD-informed EXAFS clearly shows that uranium(VI) substitutes for Fe(III) in regular structural sites by adopting a uranyl-like configuration with bent trans-dioxo bonds and axial U-O distances at about 1.95 Å.[3] This configuration is accommodated by two partially protonated Fe(III) vacancies at opposite nearest-neighbor corner-sharing sites. However, a large proportion of adsorbed uranyl was also present. Atomic resoluton scanning transmission electron microscopy was consistent with incorporation of U in structural sites associated with vacancies, and also suggests that recalcitrant adsorbed uranyl is occluded in nano pores.

Likewise, AIMD-informed EXAFS was used to detail the coordination environments Zn incorporated in hematite. In contrast to a prior study[4] claiming that Zn assumed tetrahedral coordination, AIMD-informed EXAFS showed that Zn was primarily in octahedral coordination that largely mimicked hematite symmetry but assumed a mixture of configurations that involved oxygen and protonated Fe vacancies, and no vacancies plus one proton for charge neutralization. The proportion of configurations was sensitive to synthesis conditions and responded to high temperature annealing and reductive recrystallization in unexpected ways.

Lastly, AIMD-informed EXAFS was able to put a low ceiling on the concentration of U(VI) incorporated into goethite grown by OA. The difference in solubility of U(VI) in hematite (~ 1 atom %) versus U(VI) in goethite (~0.02 atom %) can be attributed to the inert uranyl oxygens being accommodated in the hematite structure by the creation of trans corner sharing Fe vacancies along the [2,1,1] direction whereas no comparable structure is present in goethite.

References

1 Marshall et al. (2014) Environ. Sci. Tech. 48, 3724-3731.
2 Ilton et al. (2012) Environ. Sci. Tech. 46, 9428-9436.
3 McBriarty et al. (2018) Env. Sci. Tech. 52, 6282-6290.
4 Frierdich and Catalano (2012) Env. Sci. Tech. 46, 1519-1526.
5 Bylaska et al. (In Review) Env. Sci. Technol.
6 Soltis et al. (In Review) Env. Sci.: Nano

Density-Functional Tight-Binding for Geochemical Simulations: Recent Progress in Method Development and Geochemical Applications

Stephan Irle,[1,2] Ke Yuan,[1] Larry Anovitz,[1] Andrew Stack[1]
Oak Ridge National Laboratory, [1]Chemical Sciences Division and [2]Computational Sciences and Engineering Division

Advancing the density-functional tight-binding method for geochemical applications

The density-functional tight-binding (DFTB) method is an approximate version of density functional theory (DFT) and ideal to perform long timescale molecular dynamics simulations with explicit inclusion of electronic structure. We recently ported the open-source DFTB+ code to the Summit supercomputer, and using all six GPUs on a node achieved a speedup factor of 15.3 over one CPUs running 42 threads (~8 mins for an energy and gradient calculation containing 12,000 H_2O molecules, see Fig. 1). The use of extended Lagrangian Born-Oppenheimer MD and single precision algorithms are expected to reduce this wall clock time to 20 seconds/gradient, allowing a straightforward MD simulation of 1 nanosecond within 11 days on a single node of Summit.

Application of DFTB to calculate mineral surface site acidity

The simulation of a pKa of an oxide surface is grand challenge of geochemical sciences. We performed DFTB-based metadynamics simulations for an SiO_2 (101) surface using DFTB-based, and obtained an activation energy of 47 kJ/mol for the deprotonation of the outer OH group, in reasonable agreement with experimental pKa estimates of ~8. We further studied the libration modes of water molecules in bassanite ($CaSO_4 \cdot 0.4\ H_2O$), for which neutron diffraction experiments showed considerable tunneling. Our estimate by DFTB, confirmed by the DFT first principles method, is 1.3 kJ/mol, consistent with the occurrence of tunneling.

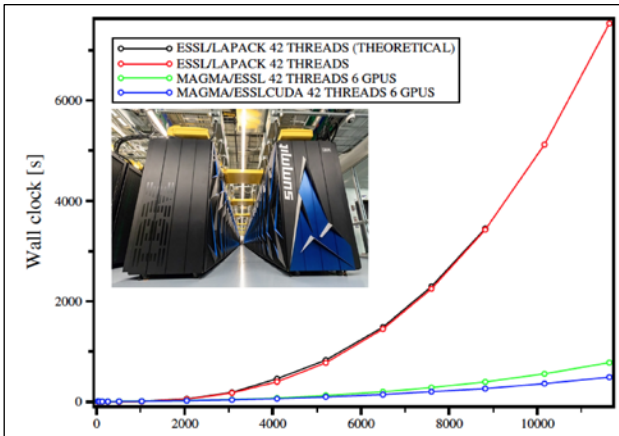

Fig. 1. Total wall clock time for DFTB energy and gradient calculation, 42 threads = 2 CPUs.

Probing Fracture and Fault Physics with Machine Learning

Paul Johnson
Los Alamos National Laboratory
(paj@lanl.gov)

Recently we have 'listened' to faults under shear in the laboratory using acoustic sensors, and analyzed the continuous signal emitted by the fault applying machine learning (ML) techniques. By applying machine learning techniques to the acoustic data, we discovered that the fault emits signals at all times during the slip cycle, and remarkably, that instantaneous signal statistical characteristics are a *fingerprint* of fault frictional state. Moreover, the statistics of the continuous acoustic signal identified by machine learning can inform of us the timing of an upcoming failure event—a laboratory earthquake or a laboratory slow slip event. This signal was discarded as noise previous to applying the machine learning approach, but it turns out to be the most important signal recorded. This is a powerful example of how machine learning can help overcome scientific bias and lead to unexpected results.

In order to determine if what we learned in the laboratory scaled to Earth, we applied a similar approach to slow slip in Cascadia. Specifically, we asked if recorded seismic signals on Vancouver Island contained information regarding the measured GPS displacement at Earth's surface. We applied a similar ML approach developed in the laboratory and found that indeed, the recoded seismic waves contain information that are a proxy for displacement as measured by GPS. As in the laboratory, the seismic signals also contain information regarding the timing of the upcoming slip event, and that the slip signature appears to be emitted at all times rather than intermittently.

Our work suggests that the continuous signal characteristics identified by machine learning are a proxy for slip. Our hypothesis is that the continuous seismic signal is a high-fidelity proxy for slip rate as preliminary results show in Cascadia, as well as potentially frictional physics as shown in the laboratory.

There are many unknowns in this frontier of science including the precise origin of the acoustic/seismic. Establishing the origin, presence, types and significance of signals discernable with ML is a central point of our Office of Science sponsored work.

Impact of Wettability on Multiphase Flow and Granular Mechanics: Experiments, Modeling and Theory

Ruben Juanes

Many natural subsurface processes involve the interaction between multiphase flow and deformation of porous media like rocks and soils. Examples include hydraulic fracturing, induced seismicity from fluid injection, and subsidence from groundwater extraction, just to name a few. In some cases, such as soil desiccation cracks or methane venting from organic sediments, surface tension plays a fundamental role in the fluid-solid interaction.

Here, we report some recent observations on how, in these cases, the flow and deformation are strongly modulated by wettability, that is, the relative affinity of each fluid to the solid making up the porous medium. These observations are surprising and intriguing, but a mechanistic explanation has heretofore remained elusive. Here, we present a fully-coupled dynamic model of granular mechanics and multiphase flow at the pore scale, which explicitly incorporates the impact of wettability. This mechanistic model allows us to explore the rich emerging behavior as a function of different parameters, such as capillary number, contact angle, initial packing density, and grain rigidity.

Beyond the suggestive predictions of pattern formation, the model also hints at the origin of the transitions between patterns. We reconcile the rich behavior we observe in terms of a jamming transition, which opens a promising way to understand novel aspects of wet granular systems.

Kavner Abstract

Stable isotopes are sensitive indicators of the mass transport and chemical reactions that occur during electrochemical processes at the non-equilibrium boundary between oxidized and reduced phases. The goal of this research program is to develop the use of stable isotope markers to help elucidate the physical and chemical nature of a reactive redox interface between solid and fluid. In this presentation, we present simplified models of an electrochemical interface based on the Marcus model, and use this to predict of temperature-dependent isotope fractionation during single electron transfer reactions. Dimensionless parameters coupling the mass transport kinetics with the chemical kinetics are introduced and discussed. Finally, we review previous experimental results, and discuss strategies and approaches for the next set of experimental tests.

Molecular-Scale Controls on Heterogeneous Nucleation and Growth of Carbonates at Mineral/Water Interfaces

S.N. Kerisit, S.L. Riechers, S.T. Mergelsberg, Graham T.R., O. Qafoku. M.P. Prange, E.S. Ilton, K.M. Rosso

Pacific Northwest National Laboratory

Current geochemical modeling paradigms for reactive fluid flow often rely solely on bulk thermodynamics. However, this approach overlooks the vastly different outcomes that can result when heterogeneous nucleation and growth pathways become kinetically favored and coating phases develop that control the chemistry of the aqueous phase. Among these poorly understood processes are nonclassical pathways of mineral growth, which add complexity to accurate description of geochemical phenomena at the field scale. One line of research in the Geochemistry program at PNNL therefore pursues fundamental insights into the formation of mineral coatings, with a long-term goal of developing a theoretical framework for reactive fluid flow capable of encompassing interfacial nucleation/growth reactions.

Heteroepitaxial growth of metal carbonates is an ideal model system of broad geochemical relevance. Here, we overview interfacial pathways exhibited at the nanoscale in the growth of otavite ($CdCO_3$) on calcite ($CaCO_3$), a seemingly simple system with only a 4% lattice mismatch. AFM measurements demonstrated that growth proceeded via spreading of 3D islands and 2D atomic layers at low and high initial saturation levels, respectively (Riechers and Kerisit, 2018). In the 3D growth mode, *in situ* AFM observations revealed a two-stage process in the nucleation of $CdCO_3$ surface precipitates, whereby a precursor phase was observed to initially form on the surface and subsequently undergo an epitaxy-mediated phase transformation to $CdCO_3$, which then grew epitaxially (Fig. 1A; Riechers et al., 2017). AFM observations also suggested that the precursor particles formed in solution, potentially as a hydrated amorphous phase, which then deposited on the surface (Fig. 1A). This hypothesis was confirmed by *in situ* X-ray PDF measurements performed at the APS with a mixed-flow reactor, in which a mixed Cd-Ca amorphous phase was detected (Fig. 1B; Mergelsberg et al., in prep.). AIMD simulations of amorphous Ca and Cd carbonates (Fig. 1C) are being used to help interpret the X-ray PDFs, compute Ca K-edge EXAFS spectra for comparison with literature data, and provide information on the water content of the amorphous phases. AIMD-informed EXAFS is a powerful method for extracting more information than is possible by shell-by-shell fitting (Kerisit and Prange, in review; Saslow et al., 2019).

The experiments revealed the significant anisotropic nature of both heteroepitaxial growth modes as well as their dependence on supersaturation, film thickness, and substrate topography (Riechers and Kerisit, 2018). In particular, in the 2D growth mode, feedback effects between stress and composition in the growing film caused the relative velocities of acute and obtuse steps to switch between the first and second atomic layers (Fig. 1D/1E). This phenomenon stems from significant Cd-Ca intermixing in the first layer, despite bulk thermodynamics predicting the formation of pure $CdCO_3$. Cation intermixing also enabled the heteroepitaxial growth of $MnCO_3$ on $CaCO_3$, despite a 10% lattice mismatch, leading to an epitaxial solid solution with spatially-complex composition (Xu et al., 2017).

Such examples show that heterogeneous nucleation and growth of a low-solubility inorganic phase can follow nonclassical pathways like that found in homogenous aqueous conditions, extending the range of systems and conditions in which such processes are operative and requiring adaptation of reactive fluid flow models.

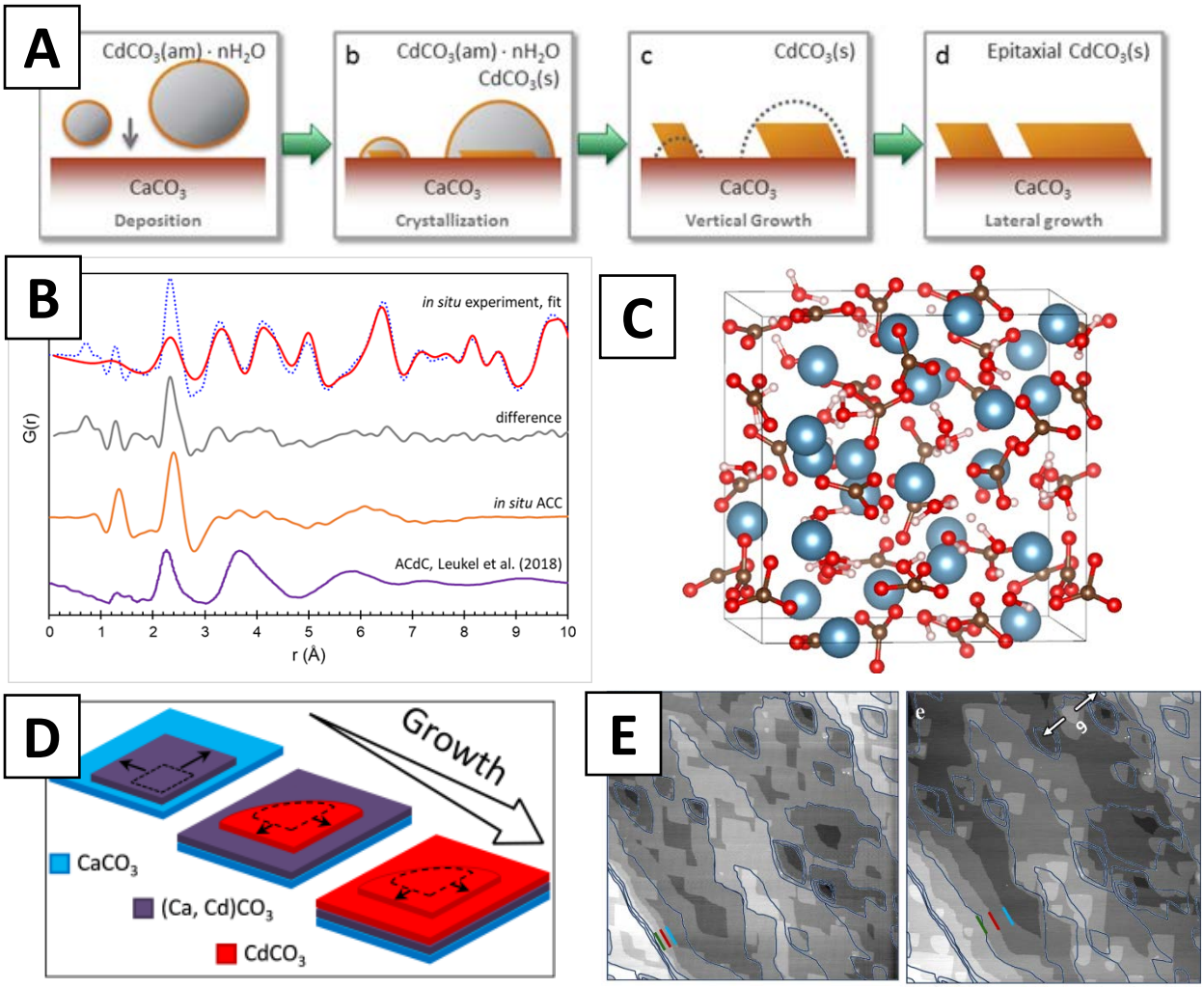

Fig. 1. (A) 3D nucleation and growth pathway of $CdCO_3$ on calcite; (B) *In situ* PDF of experiment with Cd/Ca=0.042 fitted with $Ca_{0.88}Cd_{0.12}CO_3$, difference is Cd-Ca amorphous phase with short-range order comparable to amorphous calcium carbonate (ACC) but different from amorphous cadmium carbonate (ACdC) synthesized in low water activity environment; (C) Snapshot of ACC AIMD model ($CaCO_3 \cdot H_2O$); (D) 2D growth of $CdCO_3$ on calcite: relative velocities of acute and obtuse steps switch between the first and second layers due to intermixing; (E) Topographic AFM images of 2D $CdCO_3$ growth on calcite illustrating change in step velocity with film thickness.

References

Kerisit S.N. and Prange M.P. (2019) Ab Initio Molecular Dynamics Simulation of Divalent Cations Incorporation in Calcite. *ACS Earth & Space Chemistry*, in review.

Mergelsberg S.T., Riechers S.L., Graham T.R., and S.N. Kerisit (2019) X-ray Total Scattering of Mixed Amorphous Cadmium-Calcium Carbonate Phases. *In preparation.*

Riechers S.L and Kerisit S.N. (2018) Anisotropic Growth of Otavite on Calcite: Implications for Heteroepitaxial Growth Mechanisms. *Crystal Growth & Design* 18, 159-170.

Riechers S.L., Rosso K.M., and Kerisit S.N. (2017) Nucleation and Epitaxy-Mediated Phase Transformation of a Precursor Cadmium Carbonate Phase at the Calcite/Water Interface. *Journal of Physical Chemistry C* 121, 5012-5019.

Saslow S.A., Kerisit S.N., Varga T., Johnson K.C., Avalos N.M., Lawter A.R., Qafoku N.P. (2019) Chromate Effect on Iodate Incorporation into Calcite. *ACS Earth & Space Chemistry*, in press.

Xu M., Riechers S.L., Ilton E.S., Du Y., Kovarik L., Varga T., Arey B.W., Qafoku O., and Kerisit S.N. (2017) Manganese-calcium intermixing facilitates heteroepitaxial growth at the (10−14) calcite-water interface. *Chemical Geology* 470, 152-163.

Dissolution at the pore scale: comparing simulations and experiments

Anthony Ladd, Vitaliy Starchenko, Filip Dutka, and Piotr Szymczak

University of Florida

Flow and transport in porous media is usually modeled at the Darcy scale, where the system is comprised of representative elementary volumes (REV's) described by average properties such as permeability, dispersion coefficients, and reactive surface area. Although this allows large volumes to be simulated efficiently, there are serious difficulties in developing suitable models for the properties of the REV's. When dissolution is rapid, for instance when brine pressurized with CO_2 encounters calcite, even the validity of the averaging process is called into doubt by the strong gradients in concentration within a single REV. Pore-scale modeling overcomes many of the limitations of Darcy-scale models, albeit at much greater computational cost. Nevertheless, it is not yet clear that a single set of parameters – fluid viscosity, ion diffusion coefficients, and surface reaction rates – can consistently describe the dissolution of samples with different pore structures. Here we present preliminary results of comparisons between numerical simulations of the dissolution of a soluble cylinder and microfluidic experiments.

The numerical simulations used a finite-volume discretization, with an unstructured mesh that conforms to the shape of the dissolving object. By exploiting the intrinsic separation of time scales between transport and dissolution, precise simulations can be carried out with limited computational resources. We used the OpenFOAM toolkit with customized libraries to support mesh motion and relaxation around the dissolving object. Simulations take a few hours, in comparison with one month for the laboratory experiments.

We will present results showing that the simulations can account for the time-dependent size and shape of the dissolving gypsum (see Fig. 1), with discrepancies that are within the uncertainties of the experimental measurements. The only adjustable parameter in these comparisons is the surface reaction rate. We took a value of $k = 1.125 \times 10^{-2}$ mm/s, about 2.5 times larger than typically found for single crystals, but consistent with rate-constant measurements on similar samples (P. Szymczak, Private Communication). In the course of these comparisons we made two important discoveries. First that it is essential to use pure (>99.5%) $CaSO_4$; plaster of Paris has much slower (by a factor of 2) dissolution kinetics. Dissolution in this geometry is largely transport limited – it is then essential to correct for the effects of charge-induced suppression of the ion diffusion. Here we used a Debye-Huckel correction to the diffusion coefficient, parametrized against calculations made with PHREEQC.

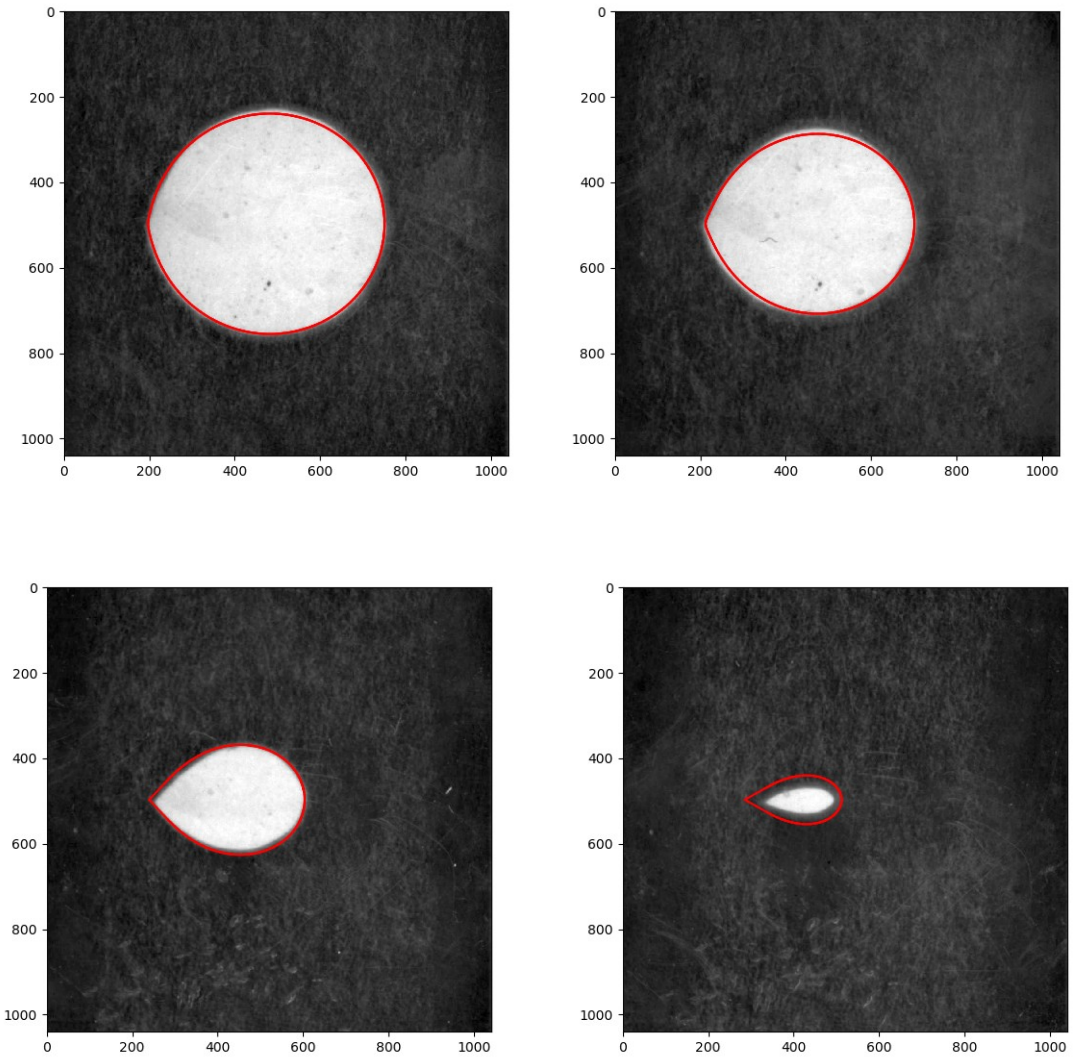

Figure 1: Shapes of a dissolving gypsum chip from microfluidic experiments (white area) and numerical simulations (red outline): times are 171, 343, 514, 643 hours. The rate constant in the simulation (~10^{-2} mm/s) is consistent with recent experimental measurements on similar samples.

V. Starchenko and A. J. C. Ladd. *The development of wormholes in laboratory scale fractures: perspectives from three-dimensional simulations.* Water Resources Res., 54:7946-7959, 2018.

This work was supported by the U.S. Department of Energy, Office of Science, Office of Basic Energy Sciences, Chemical Sciences, Geosciences, and Biosciences Division under Award Numbers DE-FG02-98ER14853 and DE-SC0018676, and by the National Science Center (Poland) under research Grant No. 2012/07/E/ST3/01734.

Progress on understanding structure-composition feedbacks in clay-rich materials

Laura Nielsen Lammers, Michael Whittaker, Nithya Subramanian, Piotr Zarzycki, Carl Steefel, Jillian Banfield, Benjamin Gilbert; Lawrence Berkeley National Laboratory; University of California, Berkeley

Subsurface storage of fossil, nuclear, and renewable fuels and the pernicious byproducts of fuel consumption requires the presence of a low permeability seal or caprock, which usually consists of clay mineral-rich geomaterials. Several characteristics of clay minerals make them ideal for inhibiting subsurface mass transport: they are layered nanoparticles generating low permeability; they possess structural charge leading to both cation adsorption and attenuation of anion transport; and they can swell, enabling self-sealing. For swelling clays, the chemical environment of the pore fluid is tightly coupled to the clay interlayer structure and hydration (swelling) state, and vise-versa. These feedbacks between chemistry and structure have made it notoriously difficult to build predictive reactive transport models for clay-rich environments. Progress in understanding clays has been severely limited by our inability to image the clay interlayer structure at sub-nm resolution or chemical/structural changes at sufficiently high temporal resolution. On the other hand, recent developments in low-dose electron microscopy and ultrafast spectroscopic tools, combined with complementary molecular simulation techniques, are poised to revolutionize our understanding of swelling clays, and of layered nanomaterials more generally.

Our project objective is to develop a multiscale model for mass transport through clay rich materials, beginning with the smallest single layer to particle aggregate scales and working towards predicting bulk properties via mesoscale modeling. We are combining high temporal resolution small angle X-ray scattering with atomic resolution cryo-TEM imaging and molecular simulation to develop a new theoretical framework for smectite clay swelling. X-ray scattering data show that in saturated KCl and NaCl electrolytes, smectite (Wy-montmorillonite) adopts a dynamic equilibrium distribution of coexisting stable hydration states that includes 2- and 3- water layer crystalline hydrates as well as osmotic hydrates, each with a distinct characteristic interlayer composition. Complementary cryo-TEM images show for the first time that individual water layer states are completely phase separated (e.g. not interstratified) in saturated solutions. Moreover, some preliminary imaging data reveal the surprising observation that interlayer ion positions in water saturated Na-montmorillonite have a high degree of lateral ordering not previously predicted by molecular simulations. We use the measured variation in layer state populations with changing ion concentrations to determine the equilibrium distribution of swelling states as a function of water and ion activities. Both an increase in aqueous K/Na and a decrease in water activity drives water desorption, shifting the distribution of layer states towards lower hydration numbers. The resulting thermodynamic model can be used to predict clay properties including bulk ion exchange selectivity, disjoining pressure, and equilibrium density as a function of water and ion activities.

Ongoing work focuses on expanding our experimental dataset for the alkali and alkaline earth metals and on providing a physiochemical basis for thermodynamic modelling using molecular simulations. We are using our cryo-TEM data to inform our simulated clay structures, with a goal of predicting excess free energies of mixing in real mixed-layer state, mixed-ion clays. Our initial results underscore the observation that clay particle disjoining pressures overestimate macroscopic swelling pressures, likely because they do not account for off-axis particle orientations characteristic of clay aggregates. Future efforts will focus on the development of a mesoscale model for clay that will enable up-scaling of clay aggregate predictions to macroscopic clay rich systems.

Multivalent Cation Adsorption on a Charged Mineral – Water Interface

Sang Soo Lee,[1] Ke Yuan,[1] Neil C. Sturchio,[2] and Paul Fenter[1]

[1] Chemical Sciences and Engineering Division, Argonne National Laboratory, Lemont, IL 60439
[2] Department of Geological Sciences, University of Delaware, Newark, DE 19716

Ion adsorption on charged mineral surfaces is central to a variety of geochemical reactions in natural environments. A robust understanding of this interfacial process can provide an insight into the fate and transport of contaminants and nutrients in aquifers and surface waters. The structure of cations adsorbed on various mineral – water interfaces has been studied using *in situ* high resolution X-ray reflectivity. Systematic studies of the adsorption of a series of monovalent and divalent cations on the negatively charged basal surface of muscovite mica have revealed that ion hydration controls the adsorbed cation speciation and energetics [1–4]. However, the molecular-scale structure of multivalent cations adsorbed at the mineral – water interface is less well understood because of their complex aqueous chemical speciation [5–6].

Here, we explore the adsorption of multivalent cations, Al^{3+} and Zr^{4+}, at the muscovite mica (001) – water interface. The aqueous chemistry of the soft metal ion Al^{3+} is largely determined by its hydrolysis that controls the molecular structure and charge of dissolved Al species. In 1 mM $AlCl_3$ solution at acidic pH values, we observed the epitaxial growth of gibbsite films at the interface even from solutions undersaturated with respect to gibbsite [7–8]. In contrast, no films were observed in basic $AlCl_3$ solutions even though the solutions were supersaturated with respect to gibbsite [8]. These results indicate that adsorption and accumulation of cationic Al(III) species (i.e., Al^{3+} and $AlOH^{2+}$ at acidic pH) is a critical step for the formation of secondary minerals on the negatively-charged mica surface (Fig. 1a). In comparison, the hard metal cation Zr^{4+} is known to form well-defined polynuclear (hydr)oxo clusters whose structure and charge are influenced by the dominant anion in acidic solution. Our studies were designed to understand how Zr–anion speciation influences ion–mineral interactions at fixed Zr concentration (= 0.1 mM), pH (= 3), and ionic strength (100 mM). In Zr solutions containing ClO_4^- or Cl^-, Zr adsorption on the mica surface occurs mainly as small oligomeric species that form a ~2 nm-thick layer on the surface whereas in SO_4^{2-} solutions Zr uptake occurs predominantly as larger nanoparticles (~5 to 15 nm tall and 20 to 40 nm wide) (Fig. 1b). The highest Zr coverage is observed in the SO_4^{2-} system, indicating that adsorption of Zr nanoparticles promotes the overall Zr uptake on the mica surface. In contrast to these results, the measurements unequivocally show no significant Zr sorption in HPO_4^{2-} solutions, consistent with the expectation that the strong chemical binding of the (bi)phosphate ions to cationic Zr species leads to the formation of neutral or negatively charged Zr species [9]. These results demonstrate the significant impact of solution chemistry on the adsorption affinity and mechanism of multivalent cations on the negatively charged mica surface.

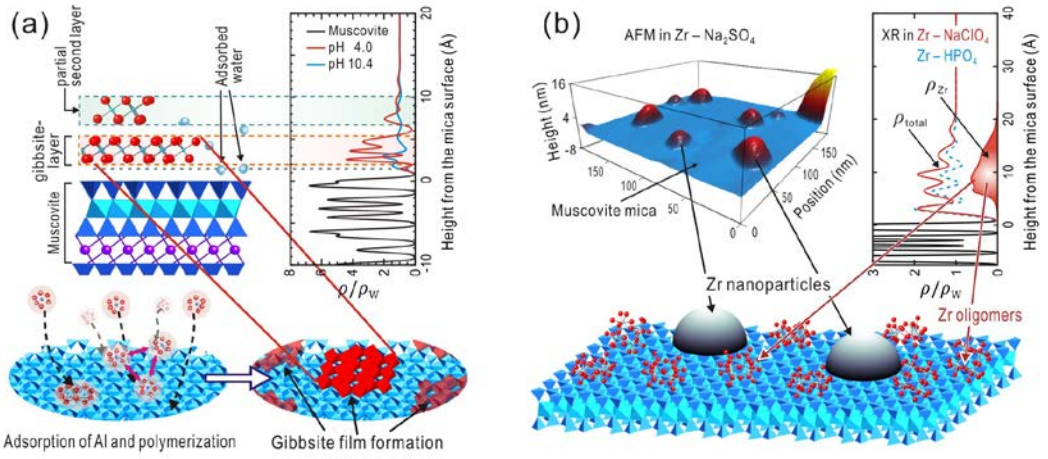

Figure 1. (a) Interfacial structure at the muscovite mica (001) – 1 mM $AlCl_3$ solution interface at pH 4.0 and 10.4. The electron-density profile at pH 4.0 indicates adsorption of Al and formation of an epitaxial gibbsite-layer film at the interface whereas no film was observed at pH 10.4. **(b)** Interfacial structure at the muscovite mica (001) – 0.1 mM Zr solution interface at pH 3 in 40 mM Na_2SO_4, 100 mM $NaClO_4$, and 45 mM Na_2HPO_4. Zr uptake occurs mostly as larger nanoparticles in the Na_2SO_4 solution whereas mostly as smaller oligomeric Zr species in the $NaClO_4$ solution. No Zr adsorption was observed in the Na_2HPO_4 solution. The distribution of adsorbed Zr nanoparticles was observed by atomic force microscopy (AFM). The total and Zr-specific electron density profiles (ρ_{total} and ρ_{Zr}, respectively) were determined by high-resolution X-ray reflectivity (XR) and resonant anomalous XR. The electron density is normalized to the density of water (ρ/ρ_W).

References:

[1] Lee S.S., Fenter P., Park C., Sturchio N.C., Nagy K.L. *Langmuir* **26**:16647-16651 (2010).

[2] Lee S.S., Fenter P., Nagy K.L., Sturchio N.C. *Langmuir* **28**:8637-8650 (2012).

[3] Lee S.S., Fenter P., Nagy K.L., Sturchio N.C. *Geochim. Cosmochim. Acta* **123**:416-426 (2013).

[4] Lee S.S., Fenter P., Nagy K.L., Sturchio N.C. *Nat. Commun.* **8**:15826 (2017).

[5] Schmidt M., Lee S.S., Wilson R.E., Soderholm L., Fenter P. *Geochim. Cosmochim. Acta* **88**:66-76 (2012).

[6] Schmidt M., et al. *Environ. Sci. Technol.* **47**:14178-14184 (2013).

[7] Lee S.S., et al. *Langmuir* **32**:477-486 (2016).

[8] Lee, S.S., Fenter, P., Schmidt, M., Sturchio, N.C., Nagy K.L. *J. Phys. Chem C*, 123:6560-6571 (2019).

[9] Yuan, K., Bracco, J.N., Schmidt, M., Soderholm, L., Fenter, P., Lee, S.S. *J. Phys. Chem C*, in press (DOI: 10.1021/acs.jpcc.9b02894).

“Sensing and Imaging Porous Media at Speed using Information-Theory in 4D and Fused Thermoacoustic, Electromagnetic, and Acoustic/Seismic Wavefields”

Accurate predictions of fluid flow, mass transport and reaction rates critically impact the efficiency and reliability of subsurface exploration and situation awareness. Quantitative dynamical sensing and imaging can play a pivotal role in the ability to make such predictions. In pursue of this, the overarching goal of this research program is to gain knowledge on the theory and experimental validation of a new information-theory-based unified sensing methodology for coupling electromagnetic (EM), acoustic/seismic (AC/S), and novel thermoacoustic (TA) physical fields, which handles multi-physics and multi-scale material characterization and underground imaging of fluid flow in porous media.

Over the last year, our research team investigated how information-theory principles can be used to design a 4D-coded dispersive meta-material (i.e. artificial structures having negative density or/and compressibility) capable of increasing the amount of information that is transferred between sensors and imaging domain per unit of time. The combination of this 4D-coding scheme with compressive sensing techniques reduces the number of receivers needed to produce images with high-spatial-resolution in both range and cross-range directions. The imaging can be performed in quasi-real-time by using our distributed Alternating Direction Method of Multipliers (ADMM) algorithm, which is capable of imposing in a distributed fashion regularizers of the form *p-norm* raised to the *q-power*. Solutions to the latter problem demonstrate, for the first time, that conventional activation functions used by Deep Convolutional Neural Networks are natural solutions to the consensus step in our space/time distorted ADMM algorithm; and, therefore, it provides a mathematical framework to understand the limitations and assess performance of state-of-the-art deep learning algorithms.

Over the last funding period, we have experimentally demonstrated that TA imaging can be used to retrieve water saturation and temperature profiles in porous media. Specifically, the injection of water in a gas-filled porous medium changes the intrinsic properties that govern the generation and propagation of the TA wave. These include but are not limited to the following: acoustic impedance and compressibility; electric conductivity, dielectric permittivity and permeability; heat capacity and volumetric thermal expansion coefficient. Our experiments compared the TA images of dry and saturated sand samples, and they showed that the TA signal amplitude increases with the water saturation level, thus the relationship between saturation level and TA signal amplitude can be established. On a second set of experiments, we demonstrated that the intensity of the TA signal depends on the temperature of the sample; suggesting that TA imaging has the potential to be used to monitor reaction rates at distance and in 4D.

[1] Chang Liu, Xu Mao, Juan Heredia Juesas, Ali Molaei, and Jose Martinez Lorenzo. “Preliminary Results of Microwave-Induced Thermoacoustics Imaging in Geological Media,” ASME IMECE 2019

[2] Xu Mao, Chang Liu, Juan Heredia Juesas, Ashkan Ghanbarzadeh-Dagheyan, and Jose Martinez Lorenzo, “Thermoacoustic Compressive Imaging Using A Resonant Metamaterial Array”, to be submitted

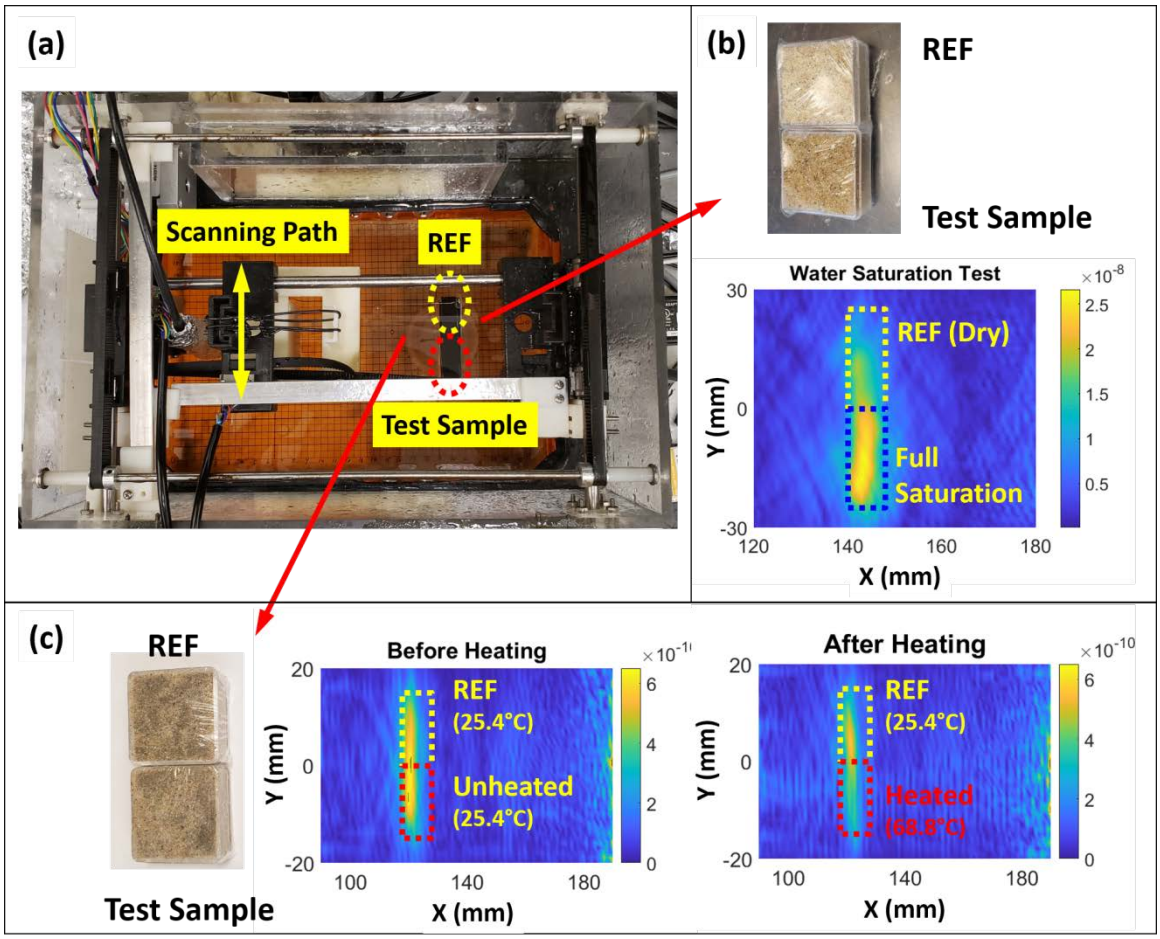

Figure 1. Tests with original prototype. (a) Top view, (b) Water Saturation test, (c) Temperature test.

Influence of Nanoconfinement on Interactions and Relaxation Dynamics of Geocolloids

Yuanzhong Zhang, Steve Merriman, and **Younjin Min**

Department of Chemical and Environmental Engineering, University of California, Riverside

Abstract

Geocolloids, which are nanoparticles formed from defragmentation and fracture of minerals and rocks, are known to ubiquitously exist in natural groundwaters and other geological systems. Field studies have reported that geocolloids can act as a third phase and increase/facilitate the transport of energy-related contaminants in waterbodies. Accordingly, a fundamental understanding of geocolloidal transport is essential to better assess and mitigate the impacts of energy production and isolation of energy system wastes on subsurface geological environments.

In this work, monodisperse silica nanoparticles with a radius of 50 nm was synthesized and utilized as model geocolloids to study the role of nanoconfinement on the dynamics, interactions, and transport properties of geocolloids. We relied on the Surface Forces Apparatus (SFA) to measure collective surface forces arising between confining mica surfaces (i.e. model geosurfaces) across colloidal dispersions of silica nanoparticles at varying degrees of confinement and environmental conditions. For the case of pure water, electrostatic repulsion started around 40 nm regardless of concentrations of silica nanoparticles (0, 0.01, and 0.1 wt.%). All measured forces arising between mica surfaces across silica nanoparticle suspension in pure water appear to be well captured by Poisson-Boltzmann (PB) theory on approach, which become attractive upon separation, giving rise to the adhesive instabilities (jumps-out) with adhesive forces of ~ 50-60 mN/m. On the other hand, in the presence of 0.1 M KCl in colloidal suspension, much long-ranged repulsion was observed where the onset of repulsion significantly increased, starting from about 300 nm - 1μm which appear to be strongly concentration-dependent of silica nanoparticles and no longer follow PB prediction. When silica nanoparticles were confined to a gap of several colloidal diameters between mica surfaces, a noticeable increase in viscosity of 2-3 orders of magnitude from the one in bulk was observed, which can be attributed to the overlap of the density distribution function and potential mean force characteristics of intermolecular interactions in confined fluids. We anticipate that our results provide a picture of the complex colloidal dynamics and interactions between geosurfaces across geocolloidal suspensions, in particular, highlighting the impact of nanoconfinement and colloidal stability manipulated by salts as well as colloidal populations.

Non-Invasive Static Fracture Characterization Based on Data-Driven Analysis of Ultrasonic Measurements

S. Misra*, H. Li, A. Chakravarty, O. Osogba
Mewbourne College of Earth and Energy, University of Oklahoma

Three sequential applications of data-driven methods on laboratory/subsurface geophysical measurements for non-invasive static fracture characterization are investigated:

Study #1*: Unsupervised outlier detection for developing robust geophysical data-driven models*

Detection of outliers is crucial for developing robust data-driven models. We investigate the performances of 4 unsupervised outlier detection techniques (ODTs), namely Isolation Forest, One-Class SVM, Local Outlier Factor and DBSCAN, on various original and synthetic well-log datasets. The unsupervised ODTs are evaluated using precision-recall curve, AUC score, and receiver operating characteristic (ROC) curve. Isolation Forest is the best performing unsupervised ODT for detecting various types of outliers. Efficient feature engineering/selection improves outlier detection.

Study #2*: Clustering of shear waveforms to spatially characterize geomechanical alteration in geomaterial*

Unsupervised clustering methods, namely DBSCAN, agglomerative, and K-means, are used to process laboratory-based ultrasonic shear-waveform measurements on Tennessee sandstone after hydraulic fracturing. Based on displacement discontinuity theory, each cluster label determined by the clustering method is then associated with a specific degree of geomechanical alteration (change of stiffness) in geomaterial due to hydraulic fracturing. Use of short-time Fourier transform followed by robust scaling and principal component analysis ensures that various clustering methods generate relatively similar clustering labels. K-means clustering-based visualization of geomechanical alterations are spatially well correlated to the acoustic-emission events recorded during the hydraulic fracturing (Figure 1).

Study #3*: Classification of sonic travel times to identify spatial features of embedded fracture network*

Wave propagation interacts with mechanical discontinuities (i.e. cracks and fractures). Data-driven classifiers are developed on simulated dataset of multipoint compressional-wavefront travel times with associated labels categorically describing the static fracture network embedded in geomaterial. Such classifiers can categorize the fractured materials using only the multipoint wavefront travel times. Random forest outperforms all other classifiers in this study. As per the sonic source-sensor configuration chosen for the study, the data-driven classifiers can not effectively categorize fracture networks of different dispersions around one primary fracture orientation. Voting-based ensemble classifier has accuracy of 0.99 when categorizing fractured materials having primary fracture orientations differing by 45° despite fracture dispersion of +/-20° around the primary fracture orientation. Materials with random, unimodal, bimodal, or linear fracture distribution can be categorized at a high accuracy of 0.86. The arrival times measured by the sensors on boundaries adjacent to the boundary on which the sonic source is placed are important for classifying the fractured materials based on fracture dispersions and distributions. On the contrary, the sensors on the boundary opposite to the sonic source are important for classifying the fracture networks based on fracture orientations.

Acknowledgements

This material is based upon work supported by the U.S. Department of Energy, Office of Basic Energy Sciences, Division of Chemical Sciences, Geosciences, and Biosciences under award number DE-SC-0019266 managed by the Geosciences Research Program.

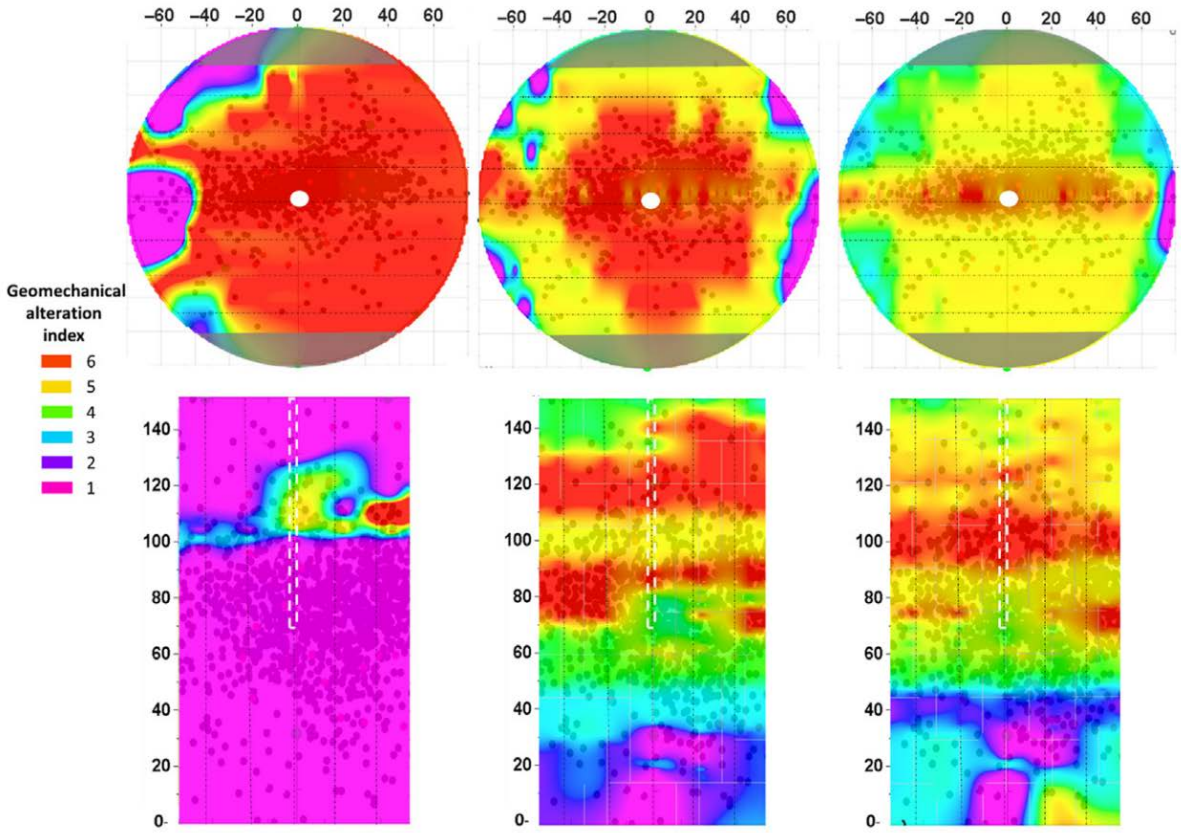

Fig. 1. Comparison of the effect of clustering method. Noninvasive visualization of geomechanical alterations in the post-fracture Tennessee sandstone sample in the axial plane (above) and frontal plane (below) obtained by DBSCAN (left), agglomerative (middle), and K-means (right) clustering of the shear-waveform dataset transformed using of short-time Fourier transform followed by robust scaling and principal component analysis. Hotter colors and larger geomechanical indices indicate larger geomechanical alteration.

Publications

Li, H., Misra, S., & He, J. (2019). Neural network modeling of in situ fluid-filled pore size distributions in subsurface shale reservoirs under data constraints. *Neural Computing and Applications*, 1-13.

He, J., & Misra, S. (2019). Generation of synthetic dielectric dispersion logs in organic-rich shale formations using neural-network models. *Geophysics*, *84*(3), D117-D129.

Upcoming Publications

Book Title: Machine Learning for Subsurface Characterization, Book, release date: 1st September 2019
https://www.elsevier.com/books/machine-learning-for-subsurface-characterization/misra/978-0-12-817736-5

Chapter 1: Unsupervised Outlier Detection Techniques for Data-Driven Geophysical Methods

Chapter 6: Unsupervised Clustering Methods for Non-Invasive Characterization of Hydraulic-Fracturing-Induced Geomechanical Alterations

Chapter 13: Non-Invasive Characterization of Fractured Materials Based on the Classification of Sonic Travel Times

Materials of the Universe - from Cosmology to Mineralogy to Materials Science

Alexandra Navrotsky

Recent discoveries of a myriad of exoplanets and of compositional and structural complexity in our solar system have started the biggest paradigm shift in geoscience (broadly defined) since the advent of plate tectonics. No longer are we, as mineralogists and petrologists, limited to thinking about the geotherm and composition of only one modest planet. Extreme conditions from screaming hot to freezing cold, from unimaginable pressure to dilute gas, abound in the universe. Planetary exploration and remote sensing yield fragmentary evidence of complex processes, past and present. This evidence and cosmochemical constraints set the stage for an unprecedented inverse problem in mineralogy and materials science - namely what assemblage of materials is consistent with the limited observations of their properties. At the same time, materials science and engineering must provide better materials and devices for both space missions and remote sensing, including sensitive spectroscopic detectors, radiation resistant materials, and efficient and durable thermal and environmental barrier coatings. These needs offer opportunities for collaboration in research and education involving mineralogy, materials science, and space science, heralding a new age of excitement and productivity in combined disciplines I call “materials of the universe.”

Chattering Dust & Architected Fracture Networks

Laura J. Pyrak-Nolte, William Braverman, Alan Wright, Harman Casey, Chven Mitchell, Nicholas Nolte and David D. Nolte
Department of Physics and Astronomy
Purdue University

Passive micro-seismic geophysical approaches use signals generated by local abrupt failure to monitor the evolution of fracture systems in the Earth's subsurface. Limitations of micro-seismic approaches include: (1) non-selective events can occur anywhere within the subsurface system, away from fractures of interest; (2) aseismic events may provide no measurable signal of fracture evolution; and (3) interpretation of events provide little or no information on fracture connectivity. Here we present a novel approach that overcomes these limitations by using transportable time-release micro-seismic granules known as "chattering dust" to map fracture flow paths. The chattering dust encapsulates compressed gas bubbles that burst concussively as the dust is chemically eroded. Unlike MEMs-based devices, the deformability of chattering dust enables them to pass through narrow constrictions in a fracture or fracture network.

In this study, we demonstrate the use of chattering dust to assess relative apertures of uniform aperture fractures under gravitational settling, to track flow paths in intersecting fracture networks, and to map fluid currents in non-uniform aperture fractures. This approach combines particle transport and chemically-induced seismicity with wave inversion to advance our ability to characterize fracture systems in the laboratory and in the subsurface.

Another key question is whether internal moving sources provided by chattering dust can be used to characterize both the connectivity of a fracture network and fractures external to the network. For hypothesis testing, this requires the fabrication of samples with fractures at known locations or that can evolve slowly in time. Traditional methods for creating fractures are often limited in terms of the location of a fracture, extent, number and connectivity. We are exploiting the geochemical-geomechanical coupling between clay and cement to develop methods to create architected fracture networks in synthetic rock, and to study geochemically-induced fracturing from volumetric changes in clay. Montmorillonite clay is known to shrink or swell in response to changes in water content. When cured clay-cement samples are dehydrated, the shrinkage of the clay induces cracks in the cement matrix. If the clay is distributed throughout the cement a dense network of fractures forms. The rate of formation is a function of the matrix strengthen and how quickly a sample can dehydrate. If the clay is localized in the form of spheres, fractures form in the matrix between the spheres. When the clay is laid out in a plane, planar fractures form after drying with apertures that range between 0.2-1.5 mm. With this new capability, individual or networks of fracture can be architected to enable studies of a much wider variety of fracture geometries that are generated in a more natural way. An important question is whether similar geo-chemically-induced cracking occurs in the field.

Acknowledgment: This material is based upon work supported by the U.S. Department of Energy, Office of Science, Office of Basic Energy Sciences, Geosciences Research Program under Award Number (DE-FG02-09ER16022).

Unraveling the Structure and Phase Transformation Pathways of Ferrihydrite

KEVIN M. ROSSO[1], ANXU SHENG[2], MICHEL SASSI[1], JUAN LIU[2], XIAOXU LIA[2], ODETA QAFOKU[1], RICHARD N. COLLINS[3], ADELE M. JONES[3], ANNE M. CHAKA[1], ERIC J. BYLASKA[1], CAROLYN I. PEARCE[1], CHONGMIN WANG[1], JINREN NI[2], ANHUAI LUD[2]

[1]Pacific Northwest National Laboratory, Richland, Washington, USA; [2]Peking University, Beijing, China; [3]University of New South Wales, Sydney, Australia

As one of the most bioavailable forms of iron, the poorly crystalline Fe(III) nanomineral ferrihydrite (Fh) plays a commanding role in geochemistry, biology, and environmental science. At ambient conditions the half-life of this metastable phase is controlled by its steady transformation to lepidocrocite (Lp) and goethite (Gt), a process limited by the low aqueous solubility of Fe(III) yet greatly accelerated by soluble Fe(II). Because the structure of Fh remains poorly resolved, and because the low solubility of Fe(III) limits aqueous mass transfer, mechanisms enabling and controlling the rate of this transformation have remained unclear for decades.

We report isolation and quantification of an overlooked labile Fe(III) intermediate at least 10 times more soluble than Fh, arising from Fe(II) oxidation on its surface, and reveal its constitutive linkage to nucleation and growth of Lp/Gt (Sheng et al., 2019). Experiments that compared time-dependent concentrations of solid-associated Fe(II) and this labile Fe(III) species against the kinetics of phase transformation assessed synchrotron-based EXAFS showed that its accumulation is directly related to product nucleation in a manner consistent with classical nucleation theory. ^{57}Fe isotope tracer experiments confirm the oxidized Fe(II) origin of labile Fe(III). For the first time, the transformation pathway as well as the accelerating effect of Fe(II) is explainable on a unified basis of the kinetics of Fe(III) olation and oxolation reactions necessary to nucleate and sustain growth of Lp/Gt products, rates of which are greatly accelerated by labile Fe(III).

Working towards corresponding structure model development, one sufficiently constrained to test this hypothesis, we also report DFT calculations aimed at predicting thermodynamically stable Fh structure prospects across a range of possible compositions determined by the amount of structural water (Sassi and Rosso, 2019a). Using on an assumed formula unit of $Fe_5O_8H+nH_2O$, we performed DFT calculations with evolutionary searching to find lowest enthalpy structures up to n=2 (equivalent to FeOOH stoichiometry). This is the most exhaustive search for the Fh structure conducted so far; more than 5000 unique configurations were generated and evaluated over five states of hydration. Among them, the Michel akdalaite model (Michel et al., 2007) was generated, along with several energetically comparable new structures at higher states of hydration. However, a direct comparison between calculated and experimental pair distribution function and X-ray diffraction patterns for the 50 lowest energy structures shows that none beyond the Michel model could be associated with Fh. Additional models that vary in terms of number of formula units per unit cell remain to be evaluated (Manceau, 2019; Sassi and Rosso, 2019b). This first exploration has already provided a novel basis for analyzing and understanding the effects of hydration and magnetism on the topology of ferrihydrite, from which we conclude that any tetrahedral Fe should be viewed as a metastable structural defect, created either as a result of the rapid kinetics of crystal growth or to accommodate a local magnetic stress between neighboring Fe atoms.

Sheng, A., J. Liu, X. Li, O. Qafoku, R.N. Collins, A.M. Jones, C.I. Pearce, C. Wang, J. Ni, A. Lu, K.M. Rosso (2019) Labile Fe(III) from sorbed Fe(II) oxidation is the key intermediate in Fe(II)-catalyzed ferrihydrite transformation. Science Advances (submitted).

Sassi, M. and K.M. Rosso (2019a). Roles of Hydration and Magnetism on the Structure of Ferrihydrite from First Principles. ACS Earth and Space Chemistry, 3, 70-78.

Manceau, A. (2019) Comment on “Roles of Hydration and Magnetism on the Structure of Ferrihydrite from First Principles”. ACS Earth and Space Chemistry, DOI:10.1021/acsearthspacechem.9b00018.

Sassi, M. and K.M. Rosso (2019b) Reply to “Comment on Roles of Hydration and Magnetism on the Structure of Ferrihydrite from First Principles”. ACS Earth and Space Chemistry, DOI:10.1021/acsearthspacechem.9b00160.

Michel, F.M., L. Ehm, S.M. Antao, P.L. Lee, P.J. Chupas, G. Liu, D.R. Strongin, M.A.A. Schoonen, B.L. Phillips, J.B. Parise (2007) The Structure of Ferrihydrite, a Nanocrystalline Material, Science, 316, 1726-1729.

Constrained Invasion Percolation Model: Growth via Leath Bursts and the Origin of Seismic b-Value

John B Rundle[1,2,3] , Ronaldo Ortez[1], Joachim Kønigslieb[1] and Donald L Turcotte[2]

[1]Department of Physics
University of California, Davis, CA

[2]Department of Earth and Planetary Science
University of California, Davis, CA

[3]The Santa Fe Institute
Santa Fe, NM

Abstract

Many driven physical processes in nature do not occur at constant rates, but rather have a burst-like character in space and time, clustering in space and time. Examples include earthquake seismicity [1], price changes price in financial markets [2], avalanche dynamics and forest fires [3], and transcriptional bursts in genomic systems [4]. In turn, many of these systems and their associated models have been mapped onto percolation models, which is a simple model for clustering [5]. An example of this type of mapping for financial markets is described in ref. [6]. An example for earthquake systems is discussed in ref. [7].

Here we discuss the invasion percolation model [8] that was originally developed to describe fluid injection into a porous medium, then apply it specifically to the problem of earthquake dynamics and statistics. Invasion percolation (IP) is a variation on the standard models of site and bond percolation [5].

Similar to the Leath method [9] in site percolation, one starts with a central seed site and grows the cluster outward. However, in the the IP model, bonds connected to existing cluster sites are opened in order of lowest probability or bond strength first, then next-lowest, and so forth. Eventually the cluster grows to "infinity" (or a pre-defined maximum size). One of the characteristics of the classical IP model is that there is only one time scale, the time scale on which bonds are progressively opened.

A variation of the standard IP model describes the invasion of a solid saturated with an incompressible fluid such as oil by another invading fluid such as water. As a result, a

pathway must always exist for the pre-existing fluid to escape. This constraint implies that a site in the model can only be connected to the origin by a single pathway. Or in other words, no point in the solid can be completely surrounded by opened bonds, for to do so would violate the incompressibility condition. This model is generally referred to as the *loopless* model, since there are no closed loops of bonds. An example for d=2 is developed in ref. [10].

To summarize our results: We propose a new model for burst-like dynamics, the constrained Leath invasion percolation (CLIP) model. We show that this model is loopless similar to the model in ref. [10]. Interpreting the percolation sites as units of energy release, we show that the model reproduces the observed natural scaling of earthquakes with the correct scaling exponent in the limit that the occupation probability equals the critical bond percolation probability in d = 2, p_{occ} = 0.5. Comparing these results to observed scaling of earthquakes in several geological regimes, we find good quantitative agreement. We conclude that the CLIP model may find significant application to earthquakes in particular, and possibly other systems with burst-like dynamics in general.

References

[1] C. H. Scholz, *The Mechanics of Earthquakes and Faulting* (Cambridge University Press, Cambridge, 2018)

[2] R. N. Mantegna and H. E. Stanley, *An Introduction to Econophysics, Correlations and Complexity in Finance* (Cambridge University Press, Cambridge, 2004)

[3] M. Paczuski, S. Maslov, and P. Per Bak , Phys. Rev. E **53**, 414 (1996).

[4] K. Bahar Halpern, S. Tanami, S. Landen, M. Chapal, L. Szlak, A. Hutzler, A. Nizhberg, S. Itzkovitz, Molecular Cell **58** (1), 147 (2015).

[5] D. Stauffer, and A. Aharony, *Introduction to Percolation Theory* (Taylor and Francis, London, 1994)

[6] D. Stauffer, and D. Sornette, *Physica A* **271**, 496 (1994).

[7] C. A. Serino, W. Klein, and K. F. Tiamp, *Phys. Rev. Lett.* **106**, 108501 (2011).

[8] D. Wilkinson, and J. F. Willemsen, *J. Phys. A: Math Gen.* **16**, 3365 (1983).

[9] P. L. Leath, *Phys. Rev. B* **14**, 5046 (1976).

Genesis, Storage, and Leakage of Shale Gas

Arndt Schimmelmann (aschimme@indiana.edu), Maria Mastalerz (mmastale@indiana.edu), and Juergen Schieber (jschiebe@indiana.edu), Indiana University, Bloomington, Indiana. U.S. Department of Energy, Basic Energy Sciences, Grant No. DE-SC0006978, 8/1/11 – 7/31/19.

Shales are important source and reservoir rocks for hydrocarbons (shale gas, oil). The three research goals of this project encompass: (1) Testing of shales' ability to generate thermogenic gas (or natural gas via catalysis) at relatively low temperatures (60, 100 and 200 °C) and different pressures (ambient, 100 MPa, 300 MPa) over months to years; (2) Quantification of the character and development of porosity in organic-rich rocks as a function of organic matter content, type of organic matter, thermal maturity, and the degree of compaction; and (3) Evaluation of the outgassing of methane from shales into the atmosphere and its potential contribution to global warming by delivering potent methane greenhouse gas.

In our study of gas generation via catalysis, we have demonstrated that low temperature (60 and 100 °C) and long-term (6 months to 5 years) heating of pre-evacuated and sterilized low-maturity shales and coals containing kerogen Types I (Mahogany Shale), II (Mowry Shale and New Albany Shale), and III (Springfield Coal and Wilcox Lignite) can yield methane volumes that are 5 to 11 orders of magnitude higher than the theoretically predicted yields from kinetic models of thermogenic methane generation (Fig. 1; Wei et al., 2018). In the absence of microbial methane generation and at temperatures not high enough for a thermogenic pathway, these results strongly suggest that generation of such volumes of methane gas involves catalytic methanogenesis. Furthermore, our experimental results suggest that catalytically generated hydrocarbons may explain the occurrence of some non-biogenic natural gas accumulations where insufficient thermal maturity contradicts the conventional thermal cracking paradigm. Extrapolation of the observed rate of catalytic methanogenesis in the laboratory suggests that significant amounts of sedimentary organic carbon can be converted to relatively dry gas over tens of thousands of years in sedimentary basins at temperatures as low as 60 °C.

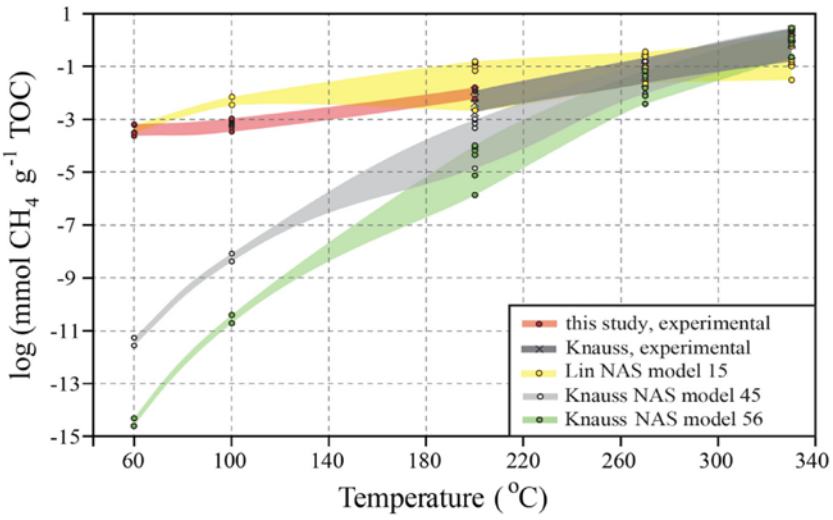

Figure 1. Cross plot of the decadal logarithm of experimentally observed and kinetic model methane yields (mmol methane g^{-1} total organic carbon (TOC) from heated New Albany Shale (NAS) *versus* temperature of experiments and model predictions (Wei et al., 2018).

In the most recent phase of the project we have examined the molecular and isotopic composition of organic matter (OM) in the Devonian New Albany Shale (NAS) to evaluate the influence of

geocatalysis on the paths and rates of transformations of sedimentary OM during diagenesis. One focus is the role of clay minerals (e.g., montmorillonite, illite, also with elevated abundances of select elements) in catalyzing diagenetic reactions that result in structural rearrangement and isomerization of key biomarkers. We utilize a suite of ten NAS samples chosen to encompass a broad maturity spectrum (vitrinite reflectance R_o from 0.39 to 1.42 %). For the two least mature samples, several biomarker indices based on diasterenes, diasteranes, steranes, and hopanes confirm the substantive influence of diagenetic reactions involving clay-catalyzed molecular transformations (Table 1). The sample suite also shows a progressive decrease in the chain-length of isorenieratane homologues with increasing maturity, a trend consistent with the expected effects of heterogeneous catalytic reactions affecting biomarker distributions. Compositional differences in biomarkers along the maturity transect serve as a baseline for evaluating results from low-temperature laboratory simulations (60-120 °C) that attempt to emulate natural conditions for abiogenic methanogenesis in shales. About 90 samples of NAS, Mowry Shale, and Second White Spec Formation shale are either ready for further analyses or in various stages of heating experiments. We aim to assess how heating of immature samples (original R_o = 0.50 %) at either 80 °C, 100 °C, and 120 °C for over one year affects the composition and isotopic signatures ($\delta^{13}C$, $\delta^{2}H$) of gases generated (CO_2, methane, ethane, and higher hydrocarbons), as well as biomarker distributions. Differences between the characteristics of biomarker ratios, R_o, gas yields, and isotopic characteristics of the newly-generated fluids *versus* source materials provide evidence of the likely mechanisms and rates of geocatalytic reactions advancing understanding of the processes involved in shale gas generation.

Table 1. Molecular indices for specific biomarker isomerization reactions in low-maturity New Albany Shale samples. R_o = vitrinite reflectance in %.

	R_o (%)	20S/(20S+20R) C_{27} diasterenes	20S/(20S+20R) C_{27} β,α-diasterenes	20S/(20S+20R) C_{29} α,α-steranes	Ts/(Ts + Tm)	22S/(22S+22R) C_{31} α,β-hopanes	22S/(22S+22R) C_{32} α,β-hopanes
IN-7	0.39	0.19	0.53	0.13	0.74	0.42	0.58
IN-3	0.54	trace	0.60	0.49	0.58	0.34	0.63

A variety of porosimetric methods, including low pressure gas adsorption, mercury porosimetry, and small-angle neutron scattering, was used to assess macro- meso- and microporosity in shales (e.g., Mastalerz et al., 2013; Bahadur et al., 2015). The results demonstrate that porosity strongly depends on the amount of organic matter and its thermal maturity. Porosity in shales at low maturity initially diminishes due to compaction, but incipient thermal cracking at the beginning of the oil window generates new porosity. Further into the oil window, the generation of additional liquid hydrocarbons fills pores and reduces the open pore space available for gas storage until the late mature stage when secondary cracking and gas generation expel some liquid hydrocarbons and open new pore spaces for gases. The influence of temperature and pressure on the evolution of porosity in shales was also tested in experiments of 6 to 12 month duration and at temperatures of 60, 100, and 200 °C, and hydrostatic pressure up to 300 MPa. While small porosity differences were noted in response to temperature increase, increase in hydrostatic pressure had no measurable effect (Mastalerz et al., 2018a). In addition, Mastalerz was invited to write a review on the significance of solid bitumen in unconventional systems for the *International*

Journal of Coal Geology, and the paper was published in 2018 (Mastalerz et al., 2018b). The paper reviews several aspects of porosity researched during this DOE-funded project and provides suggestions for future research to improve our understanding of storage and producibility of hydrocarbons from shales.

Hydrocarbon gas seepage is a significant global source of atmospheric methane, ethane and propane as greenhouse gases and photochemical pollutants. We compared the (i) regional intense natural gas seepage stemming directly from source rocks, mostly organic-rich fractured black shales in western New York State (NYS) with (ii) the areas with rare seepage in more southern regions of the Appalachian Basin and the midwestern USA (Schimmelmann et al., 2018). In addition to thermogenic methane, western NYS shale gas seeps emit ethane and propane with C_{2+3} gas concentrations reaching up to 35 vol. %. Fractures in NYS developed, reactivated and maintained permeability for gas as a result of Quaternary glaciation and post-glacial basin uplift. In contrast, more southern Appalachian and southern midwestern regions experienced less glacial loading and unloading than in NYS, resulting in less recent natural fracturing, as witnessed by the rarity of seepage on surface outcrops and in caves overlying gas-bearing shales and coals. Our survey of active gas seeps and historical literature suggests that early western NYS drilling and production of oil and gas diminished the shale gas pressure and resulted in declining gas seepage rates.

References:

Bahadur J, Radlinski AP, Melnichenko YB, Mastalerz M, Schimmelmann A (2015) Small-angle and ultrasmall-angle neutron scattering (SANS/USANS) study of New Albany Shale: A treatise on microporosity. *Energy & Fuels* **29**, 567–576. http://dx.doi.org/10.1021/ef502211w

Mastalerz M, Schimmelmann A, Drobniak A, Chen Y (2013) Porosity of Devonian and Mississippian New Albany Shale across a maturation gradient: Insights from organic petrology, gas adsorption, and mercury intrusion. *AAAP Bulletin* **97** (10), 1621–1643. http://dx.doi.org/10.1306/04011312194

Mastalerz M, Wei L, Drobniak A, Schimmelmann A, Schieber J (2018a) Responses of specific surface area and micro- and mesopore characteristics of shale and coal to heating at elevated hydrostatic and lithostatic pressures. *International Journal of Coal Geology* **197***,* 20–30. https://doi.org/10.1016/j.coal.2018.06.026

Mastalerz M, Drobniak A, Stankiewicz AB (2018b) Solid bitumen in unconventional systems: Origin, properties, and implications: A review. *International Journal of Coal Geology* **195**, 14–36. https://doi.org/10.1016/j.coal.2018.05.013

Schimmelmann A, Ensminger SA, Drobniak A, Mastalerz M, Etiope G, Jacobi RD, Frankenberg C (2018) Natural geological seepage of hydrocarbon gas in the Appalachian Basin and Midwest USA in relation to shale tectonic fracturing and past industrial hydrocarbon production. *Science of the Total Environment* **644***,* 982–993. https://doi.org/10.1016/j.scitotenv.2018.06.374

Wei L, Schimmelmann A, Mastalerz M, Lahann RW, Sauer PE, Drobniak A, Strąpoć D, Mango FD (2018) Catalytic generation of methane at 60–100 °C and 0.1–300 MPa from source rocks containing kerogen Types I, II, and III. *Geochimica et Cosmochimica Acta* **231**, 88–116. https://doi.org/10.1016/j.gca.2018.04.012

Structure and Dynamics of Branching and Looping Channels on River Deltas

John B. Shaw[1], Chris Cathcart[1], Eleni Katifori[2], Adam Konkol[2]

[1]University of Arkansas, [2]University of Pennsylvania

2019 Geosciences Research PI Meeting, Gaithersburg, MD

The growth of a river delta's channel network is a complex process that we wish to understand as a particular instance of disequilibrium growth. Advances relating a network's structure (its graph and spacing) to its dynamics (its flux partitioning and evolution) are required to improve predictions of heterogeneity in channelized sedimentary deposits. We first consider relatively simple tree (non-looping) distributary networks. We find a linear scaling between a channel's discharge and its nourishment width directly seaward of the Wax Lake Delta in Louisiana. Nourishment width is the swath of points with equal potential that receive water from the channel. Uniform water flux at this equipotential surface provides an optimality principle that organizes growing networks. This scaling and optimality is also inherent in a newly constructed model that resolves distributary network growth dynamics by coupling unchannelized flow to a moving channel network boundary (Ke et al. 2019). Channels grow at a rate proportional to water discharge at channel tips, and are therefore competing for nourishment width. A remote sensing investigation of 40 years of network growth shows that this competition occurs over multidecadal timescales on field scale deltas (Shaw et al. 2018). Nourishment widths can be estimated in 3D seismic volumes, presenting a potential tool for subsurface investigation. The results above apply for quasi-steady flows on networks without loops, and highlight the surprising lack of morphodynamic explanations for loops in coastal channel networks. We propose that loops form on river deltas at scales of spatial variations in potential. These variations occur due to due to the (a) the complex propagation of tidal waves and (b) the interaction of tides with an upstream river discharge. Loops are reproduced with numerical models developed for plant and animal vasculature, and with empirical analyses showing that the size of loops is related to the length scale at which potential (water level) covaries across a system. These findings suggest that that further study of distributary channel network morphodynamics and resulting heterogeneity may be decomposed into (i) branches and associated steady properties and (ii) loops and associated fluctuating properties.

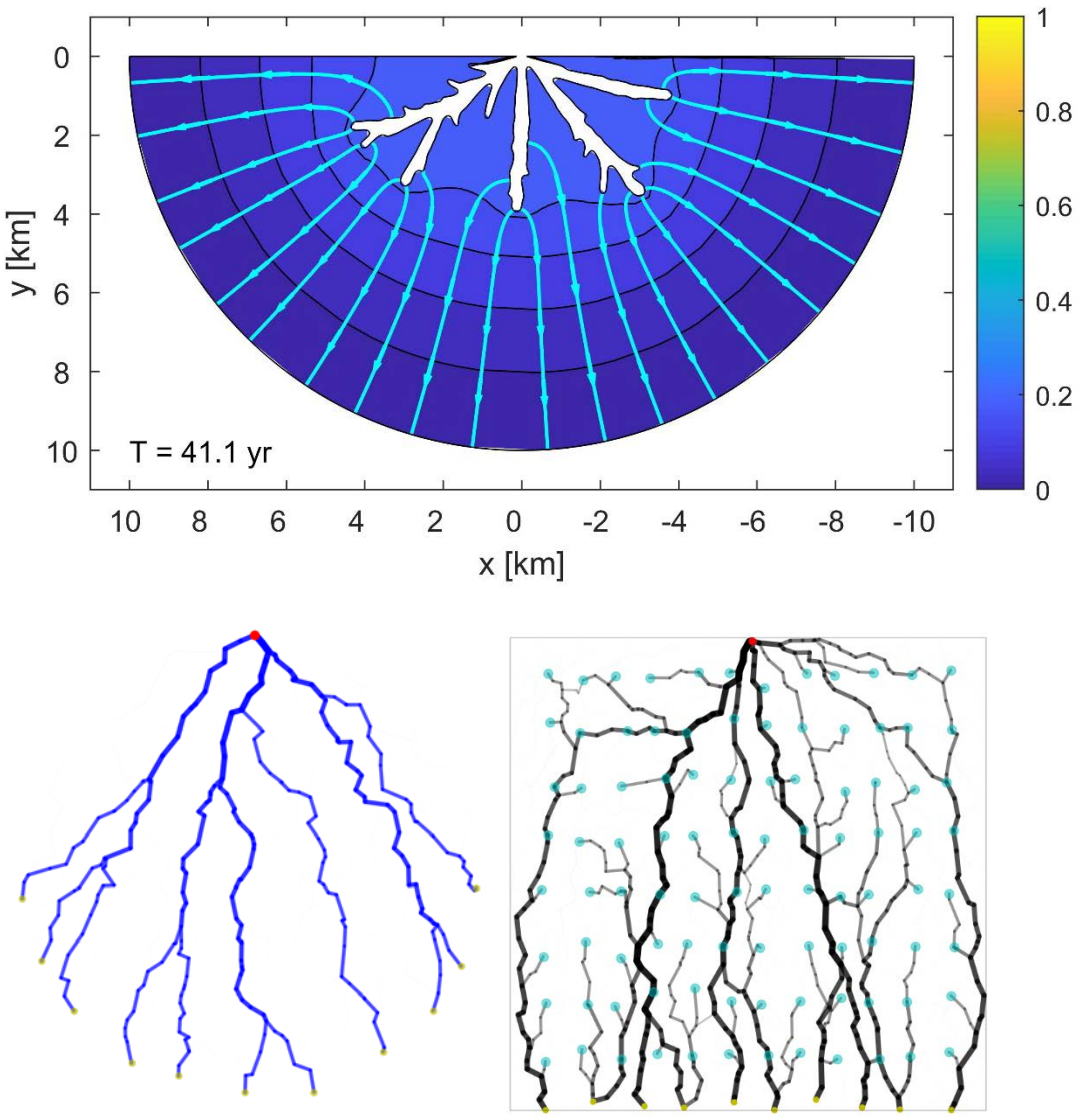

Figure: Top: Model of distributary channel network growth from Ke et al. (2019). Light blue lines are flow lines across the unchannelized domain. Channel network is white. Color bar is water surface elevation above sea level. Lower left, a steady model that grows as a tree (without loops). Lower right, when tidal fluctuation (at cyan dots) is added to river discharge (red dot), loops begin to form within the network.

Most Important Publications in the Past Year

Ke, W.-T., **Shaw, J. B.**, Mahon, R. C., & Cathcart, C. A. (2019). Distributary Channel Networks as Moving Boundaries: Causes and Morphodynamic Effects. Journal of Geophysical Research: Earth Surface, 2019JF005084. https://doi.org/10.1029/2019JF005084, **EarthArxiv**: https://doi.org/10.17605/OSF.IO/NGXF3

Shaw, J. B., Estep, J. D., Whaling, A. R., Sanks, K. M., & Edmonds, D. A. (2018). Measuring subaqueous progradation of the Wax Lake Delta with a model of flow direction divergence. Earth Surface Dynamics, 6(4), 1155–1168. https://doi.org/10.5194/esurf-6-1155-2018

New Advances in Physics-based Induced Earthquake Forecasting

Manoochehr Shirzaei
School of Earth and Space Exploration, Arizona State University, Tempe, AZ, USA

Induced seismicity linked to geothermal resource exploitation, hydraulic fracturing, and wastewater disposal is evolving into a global issue because of the increasing energy demand. Moderate-to-large induced earthquakes, causing widespread hazards, are often related to fluid injection into deep permeable formations that are hydraulically connected to the underlying crystalline basement. Here we develop and apply a physics-based model of fluid diffusion and seismicity rate to forecast the time and magnitude of the induced earthquakes. Using injection data combined with a linear poroelastic model and rate-and-state friction law, we compute the changes in crustal stress and seismicity rate in Oklahoma. We show that this model successfully forecasts large events at specific fault segments. The regional magnitude-time distribution of the observed M3+ earthquakes during 2008-2017 is reproducible. At the regional scale, the timing of predicted seismicity rate, as opposed to its pattern and amplitude, is insensitive to hydrogeological and nucleation parameters in Oklahoma. Poroelastic stress changes alone have a small effect on the seismic hazard. However, their addition to pore pressure changes can increase the seismicity rate. The injection rate reduction in 2016 mitigates the exceedance probability of M5.0 by 22% in Western Oklahoma, while that of Central Oklahoma remains unchanged. A hypothetical injection shut-in in April 2017 causes the earthquake probability to approach its background level by ~2025. We conclude that stress perturbation on pre-stressed faults due to pore pressure diffusion, enhanced by poroelastic effects, is the primary driver of the induced earthquakes in Oklahoma [*Zhai et al.*, 2019].

We further show that surface deformation data obtained from satellite SAR interferometry can be used to solve for mechanical properties of the injection layer. Focusing on the east Texas, where large volumes of wastewater are disposed at depths of ~800 m and ~1800 m, we use the datasets collected by ALOS satellite over four years before the 2012 earthquake. To solve for the hydraulic diffusivity of the injection layers, we jointly inverted the injected volume and uplift data, considering a poroelastic layered half-space. We find diffusivity values of 0.3 ± 0.1 m^2/s and 0.7 ± 0.15 m^2/s for shallow and deep injection layers, respectively, which combined with seismically-derived bulk moduli yields permeability values of $5.5 \pm 2.6 \times 10^{-14}$ m^2 and $1.9 \pm 0.25 \times 10^{-13}$ m^2 for these layers, consistent with permeability range reported for Rodessa formation and well test values. Hydraulic conductivity determines the evolution of pore pressure and thus the origin and location of induced seismicity. This study highlights the value of geodetic observations to constrain fundamental hydrogeological properties of injection layers and to monitor the evolution of the subsurface pressure change [*Shirzaei et al.*, 2019].

References:

Shirzaei, M., M. Manga, and G. Zhai (2019), Hydraulic properties of injection formations constrained by surface deformation, *Earth and Planetary Science Letters*, *515*, 125-134, doi:https://doi.org/10.1016/j.epsl.2019.03.025.

Zhai, G., M. Shirzaei, M. Manga, and X. Chen (2019), Pore-pressure diffusion, enhanced by poroelastic stresses, controls induced seismicity in Oklahoma, *Proceedings of the National Academy of Sciences*, 201819225, doi:10.1073/pnas.1819225116.

COUPLED ASSESSMENT OF SEISMIC, HYDRAULIC AND FRICTIONAL PROPERTIES OF FRACTURED ROCK TO ILLUMINATE FUNDAMENTAL PROCESSES GOVERNINGENERGY PRODUCTION AND WASTE STORAGE

Parisa Shokouhi[1], Jacques Rivière[1], Derek Elsworth[2] and Chris Marone[3]
[1] Engineering Science and Mechanics, [2]Dept. of Energy and Mineral Engineering and Energy Institute, [3]Dept. of Geosciences, The Pennsylvania State University

The ultimate goal of this project is to illuminate the fundamental processes that impact fluid permeability, local seismicity, and earthquake triggering during drilling and fluid injection. The coupled assessment of ultrasonic and hydraulic data at the laboratory scale provides physical insights into how stiffness and permeability of fractures subject to dynamic stressing are interrelated. We report on a series of laboratory experiments designed to simulate local effective stress field fluctuation and its influence on the evolution of permeability and dynamic stiffness in fractured samples of Westerly Granite and Green River Shale. L-shaped samples are loaded with tri-axial stresses to ~15 MPa and fractured in situ. Deionized water is forced to flow along the resulting fracture path by applying a differential pore pressure across the sample. Changes in the local effective stress field are imposed through normal stress or pore water pressure oscillations, with amplitudes varying between ~0.01 and ~1 MPa at frequencies in the range 0.1 to 40 Hz. A multi-channel ultrasonic data acquisition system is used to record ultrasonic data in both active and passive modes. Ultrasonic waves (center frequency of ~500 kHz) transmitted across the fracture are used to monitor the evolution of wave velocity and attenuation before, during and after dynamic stressing. The data are used to illuminate changes in elastic properties and fracture stiffness due to the imposed oscillations. The nonlinearity of fractured rock is measured in terms of three parameters: (1) the relative change (decrease) in wave velocity due to the imposed oscillations, (2) the amplitude of relative velocity change during the oscillations, and (3) the recovery rate of wave velocity post oscillation. The fracture is subsequently sheared in two 4-mm steps. During fracturing and shearing, the seismicity along the fracture is monitored passively in acoustic emission mode. Throughout the experiment, the evolution of permeability is concurrently measured to determine the relationship between fracture permeability and both elastic and inelastic properties. Finally, high-resolution laser profilometry is used to measure the roughness across the post-mortem fractured surfaces in order to reconstruct fracture aperture distribution.

Our results to date indicate that relative changes in wave velocity and permeability, due to both normal stress and pore pressure oscillations, are correlated, such that larger drops in wave velocity (higher nonlinearity) correspond to larger increases in permeability. The nonlinearity is modulated by both stress and pore pressure oscillation amplitudes. Similarly, changes in permeability are greater at higher oscillation amplitudes, although permeability enhancement is more pronounced for oscillations in pore pressure than for applied normal stresses. In addition, the measurements exhibit dependencies on the frequency of the imposed oscillations. Both nonlinearity and permeability enhancement generally increase as a function of the frequency of dynamic stressing. Finally, shearing of the fracture reduces the nonlinearity measured during normal stress oscillations for both Westerly Granite and Shale samples. After shearing, the oscillations become generally less effective in enhancing the fracture permeability.

Two mechanisms for the observed correspondence between the nonlinearity and permeability of fractures are investigated: (1) the dependence of both properties on the fracture aperture and roughness, and (2) unclogging of fracture flow conduits during water pressure oscillations. To investigate the former mechanism, the correlation between the nonlinearity and permeability change and sample thickness change is studied. The correlation is stronger for normal stress oscillations than oscillations in pore pressure. A study of permeability change versus flow rate during the oscillations does not yield a clear correlation. This suggests that unclogging is not the only mechanism behind the permeability change due to pore pressure oscillations.

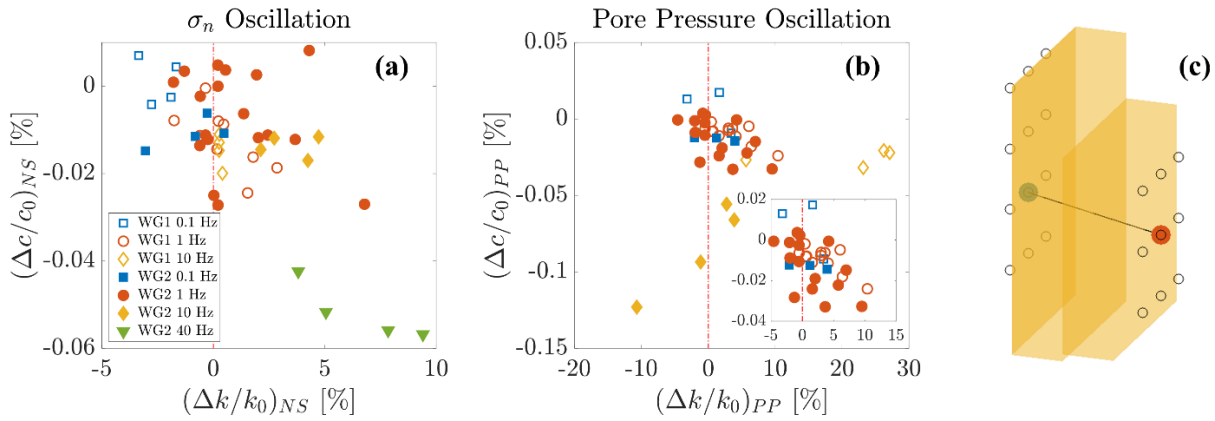

Correspondence between nonlinearity and permeability change due to (a) normal stress and (b) pore water pressure oscillations. The inset in (b) excludes the data corresponding to 10-Hz oscillations. The nonlinearity is expressed in terms of $\Delta c/c_0$, relative change in velocity due to imposed effective stress oscillations. Panel (c) shows the position of the two ultrasonic transducers used in the study relative to the fracture plane. The wavelength for a 500 kHz-pulse in Westerly Granite (~ 5000 m/s) is about 1 cm. The area probed (~ 1 cm^2) therefore corresponds to roughly 8% of the total fracture plane.

1. Shokouhi, P., Rivière, J., Guyer, R. A., & Johnson, P. A. (*2017*) "Slow Dynamics of Consolidated Granular Systems: Multi-scale Relaxation." *Applied Physics Letters*, 111, 251604.
2. *Jin, J., Riviere, J., Ohara, Y., & Shokouhi, P. (*2018*) "Dynamic Acousto-Elastic Response of Single Fatigue Cracks with Different Microstructural Features: An Experimental Investigation." *Journal of Applied Physics* 124(7), 075303 **(Editor's Picks)**
3. Shokouhi, P., *Jin, J., *Wood, C., Riviere, J., *Madara, B., Elsworth, D., & Marone, C. (*2019*) "Dynamic stressing of naturally fractured rocks: on the relation between transient changes in permeability and elastic wave velocity." *Geophysical Research Letters* (Under Review)
4. *Jin, J., Johnson, P. & Shokouhi, P. (*2019*?) "An Integrated Analytical and Experimental Study of Contact Acoustic Nonlinearity at Rough Interfaces of Fatigue Cracks." (Submitted)
5. *Jin, J., & Shokouhi, P. (*2019*?) "Data-driven Approach to Construct Quantitative Relationship between Microstructural Features at Fatigue Cracks and Acoustic Nonlinearity" (Submitted)
6. Shokouhi, P., *Madara, B., *Wood, C., Rivière, J., Elsworth, D., Marone, C. & Johnson, P. A. "Coupled Assessment of Seismic, Hydraulic and Frictional Properties of Fractured Rock." *Penn State Energy Days*, University Park, PA, May 30, *2018*. [abstract and poster presentation]
7. Shokouhi, P., *Madara, B., *Wood, C., Rivière, J., Elsworth, D., & Marone, C. "Elastic Nonlinearity of Fractured Rocks and Its Relation to Fluid Permeability." *ISNA/ICNEM*, Santa Fe, NM, July 12, *2018*. [abstract and conference presentation]
8. *Jin, J., Shokouhi, P. (July 2018) "Experimental investigation of the quantitative relationship between nonlinear ultrasonic responses and microstructure features of fatigue crack", Review of Progress in Quantitative Nondestructive Evaluation (QNDE), Burlington, VT (**Invited**)
9. Shokouhi, P., *Wood, C., *Madara, B., *Jin, J., *Manogharan, P., Riviere, J., Elsworth, D., & Marone, C. (December 2018) "Coupled Assessment of Elastic and Hydraulic Properties of Fractured Rock", AGU Fall Meeting, Washington, D.C., December 13, 2018 [abstract and conference presentation]
10. *Wood, C., *Madara, B., Shokouhi, P., *Jin, J., Riviere, J., Elsworth, D., & Marone, C. (December 2018) "The Effect of Roughness on the Elasticity and Permeability of Fractured Media", AGU Fall Meeting, Washington, D.C., December 14, 2018 [abstract and poster presentation]

*Students supervised by the PIs.

Experimental determination of mineral dissolution rates at the pore scale using microfluidic approaches

Alexis Navarre-Sitchler

Mineral dissolution plays a role in many natural and engineered earth systems, from weathering to CO2 storage permanence to fluid-rock interactions in tertiary recovery efforts for oil and gas. The rates at which minerals dissolve can be controlled by a number of factors, many of which have been studied experimentally and quantified to incorporate into numerical reactive transport models. Despite our deep understanding of the mechanisms that control rates of mineral dissolution, there remains uncertainty around applying laboratory derived rate constants to larger, field systems as a consistent discrepancy of 2-6 orders of magnitude persists between rates measured at these scales. One potential controlling factor in closing the gap between laboratory-measured and field-derived mineral dissolution rates is the role of fluid flow and hydrology. Laboratory mineral dissolution experiments are often performed under well-mixed, nearly homogeneous conditions; while field systems are often very heterogeneous with a wide range of potential fluid residence times. We have developed a method to evaluate the control of heterogeneity in fluid flow on mineral dissolution at the pore scale using microfluidic devices in reactive substrate. Fluid residence times in these devices are orders of magnitude lower previously studied. We find surface-area normalized anorthite dissolution rates similar to those previously published with pore network connectivity across the device ranging from 40-100%. We also extend the relationship between plagioclase dissolution rate and fluid residence time by two orders of magnitude, suggesting that fluid residence time exerts control on mineral dissolution rates across scales.

Effect of an Impurity on Nucleation and Growth of Barite; Implications for Porosity and Permeability Evolution in Porous Media

Andrew G. Stack[1], Juliane Weber[1,2], Vitalii Starchenko[1], Michael C. Cheshire[1], Hsiu-Wen Wang[1], Lawrence M. Anovitz[1], Stephan Irle[1], Jacquelyn N. Bracco[3,4], Paul Fenter[3], Sang Soo Lee[3], Mark Rivers[5], Joanne Stubbs[5], Peter Eng[5]

1. Chemical Sciences Division, Oak Ridge National Laboratory
2. Current address: Lunar and Planetary Laboratory, University of Arizona
3. Chemical Sciences and Engineering Division, Argonne National Laboratory
4. Current address: School of Earth and Environmental Sciences, City University of New York, Queens College
5. GeoSoilEnviroCARS, University of Chicago

The overarching goal of the ORNL Geosciences project is to attain a fundamental, predictive understanding of key chemical processes in aqueous solutions, at mineral-water interfaces and within geologic media that affect mineral nucleation, growth and dissolution, and drive changes in porosity, permeability and water. I this talk I will highlight some recent results on how a cationic impurity, strontium, has differing effects on the rates of nucleation and growth of the mineral barite ($BaSO_4$). Using synchrotron-based X-ray Computed Tomography, we observe that introduction of the impurity results in a different pore-filling behavior within porous media relative to the impurity-free solution, which will result different porosity and permeability evolution as the reaction proceeds. To begin to develop a comprehensive model that can account for these two different behaviors, we examine the effect of strontium on growth and nucleation rates of barite. For single crystal growth, we find that an independently-parameterized Lippmann diagram based on thermodynamic equilibrium assumptions fails to predict incorporation rates well. However, a process-based kinetics model is able to capture the effect of strontium on the kinetics by incorporating a known impurity-poisoning effect on step velocities coupled to a celestite-like ($SrSO_4$) morphology transition at higher strontium-to-barium ratios. We further examine the effects of heterogeneous nucleation rates of barite onto glass using optical microscopy to obtain statistical measures of nucleation rates, as well as X-ray Nano-Tomography. Overall, we find evidence that the impurity does have different effects on the rates of nucleation versus crystal growth, which will in turn determine the porosity and permeability evolution of the system as precipitation proceeds. However, incorporation of some of these specific chemical effects into macroscopic models capable of being used in a reactive transport simulation is still a work in progress.

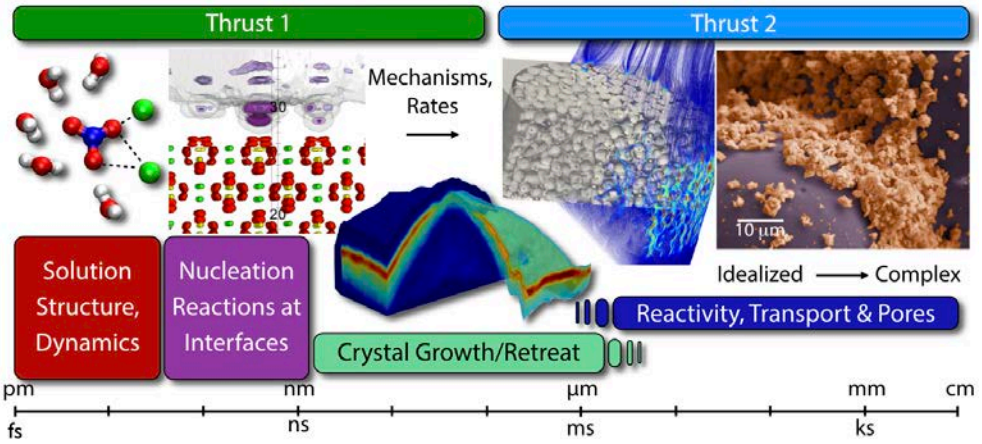

Next Generation Synchrotron X-ray Methods and Tools for Quantifying Chemical Complexity at Mineral-Fluid Interfaces

Joanne E. Stubbs, Peter J. Eng, Stephen R. Sutton
GeoSoilEnviroCARS, The University of Chicago

The GeoSoilEnviroCARS beamlines, located at the Advanced Photon Source, provide members of the geosciences community with the tools and training required to take advantage of numerous synchrotron-based analytical techniques. From its inception, the GSECARS mineral-fluid interface program has focused on molecular-scale determination of crystal termination structure, interaction with water, adsorbate conformation, and reactivity.

Current DOE Geosciences support is enabling the design and development of new tools that will dramatically expand the suite of molecular-level mineral-fluid interfacial structures and solution conditions that can be probed by synchrotron x-ray techniques such as crystal truncation rod (CTR) diffraction and resonant anomalous x-ray reflectivity (RAXR). Historically, mineral-fluid interface scattering experiments have been limited to highly idealized systems encompassing a short list of minerals that grow to form large (> 3 mm), perfect single crystals. Chemical conditions for three-dimensional atomic structural measurements have traditionally been limited to systems at chemical equilibrium and solutions that are stable in films a few microns thick. By developing new sample environments, measurement technologies, and data analysis tools this project is opening the techniques to an unprecedented range of mineralogy and chemical complexity, enabling rapid resolution of pressing scientific problems by a wide community of scientists.

We are designing and fabricating sample cells and measurement methods optimized for small crystals (< 300 microns), thus circumventing many of the constraints previously imposed on crystal size and quality, allowing us to measure surface and interfacial structures on fine-grained transition metal oxides, phyllosilicates, and other minerals previously regarded as intractable. These efforts are supported by a new sample viewing system, optimized scattering geometries, optical component modifications, and software enhancements.

In addition, we continue to engage in collaborative experiment design for complex interfacial problems relevant to the DOE mission. Recent highlights include three-dimensional characterization of epitaxial aluminum oxyhydroxide films on muscovite surfaces[1], electrochemical investigations of the hematite-electrolyte interface[2-4], beneficiation of rare earth element ores[5], and the surface reactivity and growth of barite [6, 7] – a mineral that is important in oil pipeline scale formation. We actively invite collaboration with geoscientists interested in mineral-fluid interfacial problems. Our expertise in x-ray measurements and instrument design, coupled with world class facilities, position us uniquely to support novel experiments at the leading edge of discovery.

1. Stubbs, J. E.; Legg, B. A.; Lee, S. S.; Dera, P.; DeYoreo, J. J.; Fenter, P.; Eng, P. J., Epitaxial growth of gibbsite sheets on the basal surface of muscovite mica. **In prep**.
2. McBriarty, M. E.; von Rudorff, G. F.; Stubbs, J. E.; Eng, P. J.; Blumberger, J.; Rosso, K. M., Dynamic Stabilization of Metal Oxide-Water Interfaces. *Journal of the American Chemical Society* **2017,** *139* (7), 2581-2584.
3. McBriarty, M. E.; Stubbs, J. E.; Eng, P. J.; Rosso, K. M., Potential-Specific Structure at the Hematite-Electrolyte Interface. *Advanced Functional Materials* **2018**, 1705618.
4. McBriarty, M.; Stubbs, J.; Eng, P.; Rosso, K., Reductive Dissolution Mechanisms at the Hematite-Electrolyte Interface Probed by in Situ X-ray Scattering. *Journal of Physical Chemistry C* **2019,** *123* (13), 8077-8085.
5. Stack, A. G.; Stubbs, J. E.; Srinivasan, S. G.; Roy, S.; Bryantsev, V. S.; Eng, P. J.; Custelcean, R.; Gordon, A. D.; Hexel, C. R., Mineral-Water Interface Structure of Xenotime (YPO4) {100}. *Journal of Physical Chemistry C* **2018,** *122* (35), 20232-20243.
6. Bracco, J. N.; Lee, S. S.; Stubbs, J. E.; Eng, P. J.; Heberling, F.; Fenter, P.; Stack, A. G., Hydration Structure of the Barite (001)-Water Interface: Comparison of X-ray Reflectivity with Molecular Dynamics Simulations. *Journal of Physical Chemistry C* **2017,** *121* (22), 12236-12248.
7. Bracco, J.; Lee, S.; Stubbs, J.; Eng, P.; Jindra, S.; Warren, D.; Kommu, A.; Fenter, P.; Kubicki, J.; Stack, A., Simultaneous Adsorption and Incorporation of Sr2+ at the Barite (001)-Water Interface. *Journal of Physical Chemistry C* **2019,** *123* (2), 1194-1207.

Flow rate and ionic strength effects on calcite reactivity in microchannels

Bektur Abdilla[1], Daniel Minahan[2], Sang Soo Lee[3], Jason Gleghorn[2], Paul Fenter[3] and Neil C. Sturchio[1]

[1] Department of Geological Sciences, University of Delaware, Newark, DE 19716, USA

[2] Department of Biomedical Engineering, University of Delaware, Newark, DE 19716, USA

[3] Chemical Sciences and Engineering Division, Argonne National Laboratory, Lemont, IL 60439, USA

Reactions at the mineral–water interface play a central role in geochemical processes. They control mobility and transport of dissolved ions and molecules. Minerals also serve as substrates and hosts for microbial life. Calcite, in particular, occurs widely, regulates the pH of natural waters, is a major global CO_2 sink, and is effective at metal sequestration [1 – 7]. Most studies on the reactivity of calcite have been conducted using calcite powders or freshly cleaved surfaces in contact with bulk solution. In natural environments, however, chemical reactions may occur in interconnected pore spaces, where the mineral-water interactions are controlled by advective-diffusive transport under fluid saturated conditions [8 – 10]. A proper mechanistic understanding of geochemical processes in microporous media is needed to have a validated and predictive models of the coupled evolution of hydraulic and chemical properties of geologic units (i.e. in aquifers and reservoir rocks). While the effect of fluid flow on reactive transport is well known, the reactivity of minerals under advection dominated conditions in confined pore networks is not well studied.

Here we present initial results on the effects of different fluid flow conditions and pathways on chemical and structural changes at the calcite (104)-water interface as a function of reaction progress in confined channels using a novel microfluidic apparatus fabricated directly on a calcite (104) surface (Fig. 1). The microfluidic cell controls initial composition and continuous flow rate of solutions in confinement to simulate the reactivity of a calcite in controlled microporous environment. We systematically investigated effects of flow rate, flow direction (with respect to crystallographic orientation) and solution ionic strength on calcite reactivity in a pH 3.5 lead nitrate solution. Profilometer measurements and synchrotron X-ray fluorescence mapping (both performed ex-situ) revealed that both the amount of calcite dissoluton (based on the average etching depth along the reaction channels) and the amount of deposited lead (measured by synchrotron X-ray fluorescence microprobe, measured at the GSE-CARS sector at the APS) were dependent on flow rate and ionic strength. Surpisingly, both etching depth profiles and surface lead concentrations exhibited oscillatory variations along the flow channel (Fig. 2). These results indicate complex Ca-Pb-(H)CO3 reaction pathways on a calcite (104) surface. We hypothesize that the rate limiting step in PbCO3 formation is the reaction of Pb^{2+} with HCO_3^- (whose concentration is locally increased by calcite dissolution) leading to the release of a proton and an associated increase in the local solution acidity, which creates a pH feedback loop that results in the observed oscillatory behavior. We also observed sensitivity to the flow direction, with deeper etching of the calcite surface and more deposited lead when the flow direction was oriented from acute ($[48\bar{1}]_-$, $[\bar{4}41]_-$) to obtuse sides ($[48\bar{1}]_+$, $[\bar{4}41]_+$) compared to the opposite flow direction, indicating that obtuse steps dissolve slower in these conditions.

*The X-ray fluorescence mapping was performed at the GSE-CARS sector of the Advanced Photon Source. We thank Dr. Matt Newville and Dr. Tony Lanzirotti for their assistance.

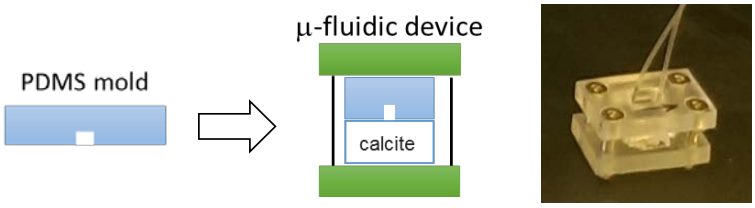

Figure 1: *(Left) Schematic cross sectional view of the microfluidic device that allows solutions to react with single crystal calcite surfaces with controlled composition, flow rate and flow direction. (Right) Photo of working cell.*

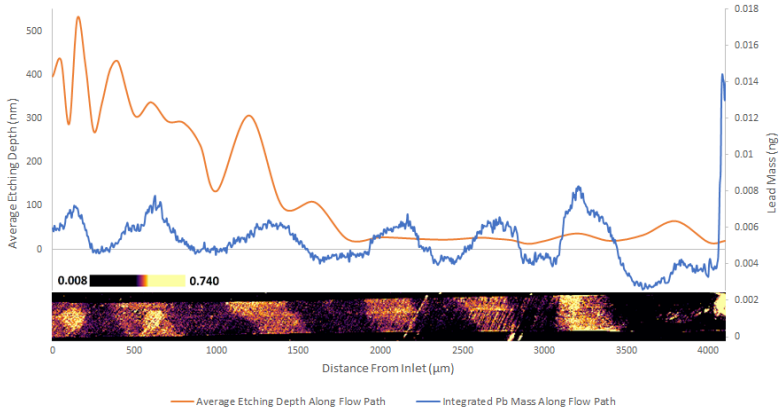

Figure 2: *(Top) Average etching depth and sorbed lead (Pb) mass (integrated across the flow channel) as a function of distance from inlet in a microfluidic channel at flow rate of 1000 nL/min. (Bottom) Spatial distribution of Pb inside the microfluidic channel measured using synchrotron X-Ray fluorescence. Color scale indicates log(Pb[ng/mm^2]) and each pixel represents a 5x5 μm^2 area.*

References:

[1] Pokrovsky O.S., Golubev S.V., Schott J., and Castillo A. *Chem. Geol.* **265**:20–32 (2009)
[2] Hagens, M., Hunter K.A., Liss P.S., and Middelburg J.J. *Geophys. Res. Lett.* **41:**935–941 (2014)
[3] Hagens M., Middelburg J. J. *Geochim. Cosmochim. Acta* **187**:334–349 (2016)
[4] Yuan K., Lee S.S., Andrade V.D., Sturchio N.C., and Fenter P. *Environ. Sci. Technol.* **50**:12984-12991 (2016)
[5] Yuan K., Andrade V.D., Feng Z., Sturchio N.C., Lee S.S., and Fenter P. *J. Phys. Chem. C* 122 (4):2238-2247 (2018)
[6] Yuan K., Lee S.S., Wang J., Sturchio N.C., and Fenter P. *Chem. Mater.* **30:**700-707 (2018)
[7] Yuan K., Starchenko V., Lee S.S., De Andrade V., Gursoy D., Sturchio N.C., and Fenter P. *ACS Earth Space Chem.* **3**:833-843 (2019)
[8] Anovitz L.M., Cole D.R. *Rev. Mineral Geochem.* **80**:61–164
[9] Stack A.G., Kent P.R.C. *Environ. Chem.* **12**:20–32 (2015)
[10] Steefel C.I., Beckingham L.E., Landrot G. *Rev. Mineral Geochem.* **80**:217–246 (2015)

Progress on fundamentals and frontiers in carbonate clumped isotope geochemistry

Aradhna Tripati
Department of Earth, Planetary, and Space Sciences, UCLA

The goal of the project is to build a solid framework from which to interpret clumped isotopic signatures in geological samples from a variety of conditions, which would improve applications to study processes as wide-ranging as carbonate biomineralization and diagenesis. We are several major knowledge gaps in carbonate clumped isotope geochemistry within the analytical, experimental, and theoretical realms. These range from fundamental questions about thermodynamic and kinetic controls on clumped isotope fractionations, to the nature of potential biases introduced from sample preparation and analysis. This presentation will discuss progress made on addressing fundamental questions in carbonate clumped isotope geochemistry, frontiers research, and what the next phase of our endeavors will focus on.

Atmosphere Processes Coupling to the Solid Earth: Quantification of Seismic Signals Emerging from Weather Related Events

Frank Vernon, Chris Johnson
IGPP, UC San Diego

Analysis of continuous seismic waveforms recorded by a temporary deployment at Sage Brush Flats on the San Jacinto fault zone reveal earthquake- and tremor-like signals generated by the interaction of wind with obstacles above the surface. Tremor-like waveforms are present at the site during wind velocities above 2 m/s, which occur for 70% of the deployment duration. The wind-related signals produce ground velocities that exceed the average ground motions of M1.0-1.5 earthquakes for 6% of the day. Waveform spectra show a modulation of the amplitude that correlates with the wind velocity and distance from local structures shaken by the wind. The earthquake-like signals are present within the tremor-like waveforms as impulsive bursts. Earthquake-like signals are found to originate from the vegetation and local structures, and are modified on length scales of 10's of meters. Transient signals originating beyond the study area are also observed with amplitudes greater than some microseismic events. The ground motions generated by the wind contribute to local high-frequency seismic noise that is different than the global ambient noise. During elevated wind conditions a borehole seismometer at a depth of 148 m shows increased energy in the 1-8 Hz band that is commonly used for earthquake and tremor detection. Some of the wind-related signals recorded by the borehole sensor may be associated with small failures of the subsurface material. The wind-related earthquake- and tremor-like signals should be accounted for in earthquake detection algorithms due to the similar features in both the time and frequency domain.

*The research was done in collaboration with Y. Ben-Zion

Forward Flux Sampling Simulations of Water Exchange Reactions on Pico- to Micro-Second Timescales

Adam F. Wallace (afw@udel.edu)
Department of Earth Sciences
University of Delaware

Molecular dynamics simulations are invaluable tools in the study of the mineral-water interface. Although standard simulation methods routinely address timescales that are sufficient to characterize relatively small-amplitude fluctuations in the structure of the interface, more infrequent large-scale fluctuations that drive events such as ion attachment and detachment typically remain under-sampled. Yet, it is these "rare events" that beg our attention, because they are ultimately responsible for the chemical behavior we observe at much longer time- and length-scales.

At present, our rare event simulation capabilities are limited by our ability to characterize complex multi-dimensional energy landscapes and to identify transition pathways between important stable and metastable states. While numerous methods have been advanced to overcome high barriers and accelerate the exploration of free energy landscapes in dynamical simulations, relatively few return kinetic information. Amongst these, path sampling methods are arguably the most promising for complex systems because they avoid the costly evaluation of the free energy landscape. Within the broader path sampling family, Forward Flux Sampling (FFS) has the additional advantage that the rate calculation need not be bootstrapped with an initial reactive trajectory. However, the efficiency of the FFS procedure is sensitive to the nature of the order parameter that is chosen to define the sampling interfaces.

The main objective of this project is to develop a variant of the FFS method that is insensitive to the order parameter specification. To meet this objective, we hypothesize that the FFS sampling interfaces may be defined in terms of the time spent outside the reactant basin rather than a geometrically defined order parameter. If so, we expect that this modification will: (1) minimize sampling bias; (2) enable sampling of multiple and/or competing reaction pathways; and (3) allow performance of unguided searches for unknown intermediate states along complex reaction pathways.

As proof of concept, the kinetics of water exchange on Li^{+} and Ca^{2+} (residence times of ~10-500 picoseconds) were obtained with FFS-time method described above and two standard direct simulation methods at 298K; namely, by integration of the time averaged residence time correlation function and direct counting. The kinetics of water exchange were also investigated on Mg^{2+}, which exhibits first shell water residence times on the order of ~2-5 microseconds. Here, an initial survey of several popular magnesium-water interaction potentials was conducted by comparing experimental exchange rates with those derived from direct simulations at 373K. For those potentials that performed reasonably well compared to experiment, further rate calculations were performed at 298K and 373K with FFS-time and reactive flux methods.

The calculated first shell water residence times for Li^{+} and Ca^{2+} obtained from the direct simulation methods were consistent with those derived from the FFS-time method. Likewise, the reactive flux and FFS-time derived Mg^{2+} water exchange rates were found to be equivalent within numerical uncertainty at both 298K and 373K. These results both demonstrate both validity of the FFS-time concept, and indicate that the method can be utilized over at least ~5-6 orders of magnitude, well into the microsecond regime.

Ion Association in Concentrated Aqueous Salt Solutions: Concentration-Dependent Reaction Dynamics

Hsiu-Wen Wang[1], Nikhil Rampal[1], Alexander Brady[1], Joerg Neuefeind[1], Denys Biriukov[2], Milan Predota[2], Andrew G. Stack[1]
[1]Oak Ridge National Laboratory; [2]University of South Bohemia

One of the continuing challenges present in salt solutions is to understand the ion association reactions that drive crystallization and the importance of solvation, complexation and solute clustering. The problems in understanding this phenomenon are exacerbated in solutions with high salt concentrations. The structure and dynamics of salt solutions extended to regions of low water activity have been increasingly recognized as important for predicting chemical reactivity for energy storage, legacy waste remediation and in highly concentrated flowback brines in shales. Obtaining a microscopic view of solvent-solute interactions at high salt concentrations allows determination of reactant encounter rates, which underlies many chemical syntheses in addition to nucleation processes. This poster will cover ongoing research focused on two chlorine-containing salt solutions at high concentrations (7.3 m $CaCl_2$ and 4.5 m $ZnCl_2$) through a combination of computational simulations and neutron diffraction with isotopic substitution (NDIS) experiments. Validation and parameterizations are made to an existing force field in order to correctly capture chloride ion solvation structure and ion-pairing formation in the Cl-NDIS pair distribution function data. Cation-specific effects are observed with no evidence of Ca^{2+}-Cl^- ion pair formation in 7.3 m $CaCl_2$ solutions as compared to $ZnCl_2$ solutions. In the latter case, ligand exchange reactions from fully solvated Zn^{2+} octahedral ($[Zn(H_2O)_6]^{2+}$:7%) to the dominating tetrahedral molecular complexes ($[ZnCl_2(H_2O)_2]^0$:24% and $[ZnCl_3(H_2O)]^-$:33%) are discussed. Comparisons of simulations in concentrated (4.5 m) and dilute (0.01 m) solutions suggests that association reaction mechanisms and thermodynamics are concentration dependent. Both water solvent and counterions control local specific bonding interactions, and the free energy barriers for the interconversions from one stable coordination state to another are increased with increasing concentrations in $ZnCl_2$ solution system. This suggests hindered reaction dynamics with ions assume locally-favored structures, but may frustrate crystal nucleation processes.

Abstract

Residual lattice strain in quartzites as a paleopiezometer

Rudy Wenk and Chase Chandler

Dept. Earth and Planetary Science UC Berkeley

If a crystal lattice is subjected to a stress, it becomes distorted and no longer represents the ideal crystal symmetry. If the stress introduces defects such as dislocations and mechanical twins, some of this distortion is preserved when the applied stress is removed. In this study we investigate lattice distortion in quartz at the micron scale with synchrotron X-ray Laue diffraction at beamline 12.3.2 of the Advanced Light Source, Berkeley. From Laue diffraction images the local deviatoric strain tensor can be derived on a 1 micron spot. The method is applied to metasedimentary quartzites from the Bergell Alps that were deformed at conditions of amphibolite and greenschist facies in Tertiary (~30 M.y.). Crystallographic orientation patterns were measured with neutrons at LANL. They suggest deformation in plane strain. Laue diffraction was applied to thin sections. The residual paleostress is represented in lattice strain pole figures and overall indicates shortening perpendicular to the schistosity plane. The new method shows promise to be used as a paleopiezometer but needs to be further tested with other samples and refining the complex experimental and analytical procedures.

Mineral Alteration of Shales by CO_2 and Brine Containing Surfactants

[1]Charles Werth, [2]Kishore Mohanty, [1]Lynn Katz, [1]David Kyungtae Kim, [2]Tongzhou Zeng

1. Department of Civil, Architecture and Environmental Engineering, University of Texas at Austin

2. Department of Petroleum and Geoscience Engineering, University of Texas at Austin

Carbon dioxide is increasingly being injected into subsurface reservoirs to fracture tight formations, enhance oil recovery, and sequester CO_2 generated from stationary power sources. Carbon dioxide used for hydraulic fracturing or enhanced oil recovery is often injected as a foam, which contains primarily CO_2, water, and one or more surfactants; natural surfactants are also present in reservoirs. Surfactants adsorb to mineral surfaces and alter mineral wettability. We hypothesize that they also protect mineral surfaces from reaction in CO_2-acidfied brines, thereby slowing mineral dissolution. To test this hypothesis, we measured reactivity of a real shale rock in a CO_2-brine mixture with and without surfactant by measuring changes in aqueous phase cation and anion concentrations. Results indicate that the presence of an anionc surfactant (interal olefin sulfonate, IOS) affects dissolution of Ca^{2+} and Mg^{2+} containing minerals. PHREEQC modeling indicates calcite is the primary mineral affected, so freshly cleaved calcite (with $\{10\bar{1}4\}$ cleavage faces) was reacted in the CO_2-brine mixture. Laser profilometry and atomic force microscopy (AFM) were used to measure etch pits in calcite at resolutions down to single nm's. Without surfactant addition, large isolated etch pits approximately 2.917 um deep were formed. With surfactant addition, many shallower etch pits approximately 0.089 um deep were formed; these shallower pits merged together over time and there was less overall dissolution. IOS adsorption results indicate that sorption is strongest to clays, but calcite adsorption is still significant and can dominate in high calcite reservoir materials. X-ray photoelectron spectroscopy (XPS) and AFM are being used to probe whether IOS sorbs preferentially to etch pits instead of freshly cleaved {1014} surfaces, thereby resulting in more shallower pits. Our results suggest that surfactants inhibit etch pit development by preferentially sorbing onto etch pit surfaces and protecting them from dissolution. The primary implication of the results is that anionic surfactants may protect calcite surfaces from reaction in the subsurface, thereby mitigating degradation of mechanical integrity in high calcite reservoirs.

Dielectric properties of the electrical double layer at mineral/electrolyte interfaces

PIOTR ZARZYCKI, CHRISTOPHER COLLA, TETSU TOKUNAGA, LAURA NIELSEN LAMMERS, BENJAMIN GILBERT

Dielectric relaxation spectroscopy is a unique probe of subtle solvent relaxation phenomena and behavior of water in various states of interactions [1,2]. However, spectra interpretation remains problematic [3,4]. Here, we show how molecular modeling can help to unambiguously decompose spectra into individual relaxation modes and relate them to the underlying physical processes of water at the mineral/electrolyte interfaces. By combining molecular modeling and experimental methods, we can explain the effect of crowding and mineral confinement on dielectric, and conductive properties of aqueous solutions. Here, we present the results obtained using classical molecular dynamics, dielectric and infrared spectroscopy and sorption and potentiometric studies of selected swelling and non-swelling clays, carbonate and silicate minerals. We conclude that the water dielectric response is governed by the interplay between solvation and hydrogen-bond network dynamics.

Our results are relevant for understanding the properties of aqueous solutions in contact with mineral surfaces, role of the electrical double layer forces, dissolution and precipitation of energy-relevant geological interfaces in the Earth surface and subsurface.

[1] Buchner, R.; Hefter, G. *Phys. Chem. Chem. Phys.* **2009**, *11*, 8984–16.
[2] Kaatze, U.; Behrends, R.; Pottel, R. *J. Non-Cryst. Solids* **2002**, *305* (1-3), 19–28.
[3] Kremer, F. and A. Schönhals Broadband Dielectric Spectroscopy. **2003**, Berlin, Springer.
[4] Raicu, V. and Y. Feldman Dielectric Relaxation in Biological Systems. **2015** Oxford, Oxford University Press.

Effect of Pore Fluid Pressure on Slip Instability Beyond Effective Stress Threshold

Wenlu Zhu and Tiange Xing

Department of Geology, University of Maryland, College Park, MD 20742

The dynamic interrelationships between rocks, pore fluids and deformation hold the key to understanding many natural processes, including fault mechanics and fault stability. In the past few years, we focus on improving knowledge of the relations between inelastic deformation and transport properties, of the effects of fluid-rock reactions on rock strength and failure, and of the detailed mechanics of pore pressure sensitive fault slip instabilities.

In a classic framework based on the elastic rebound theory, the earthquake cycle includes the interseismic period of strain accumulation and the coseismic period of sudden strain release along a tectonic fault. Fault motion is thought to be bimodal, i.e, continuous aseismic sliding during the interseismic period, or sudden rupture of a locked portion during earthquakes. The deficit of slip accumulated during the interseismic phase should be balanced by the seismic slip and aseismic creep. Discovery of slow slip events (SSEs) creates new challenges to our understanding of the mechanics of earthquakes and faulting. SSEs proceed at rates much slower than earthquakes (e.g., ~m/s) but faster than plate motions (e.g., mm to cm per year). The so-called slow events can last from a few seconds to years and radiate only low frequency elastic waves. Geophysical observations reveal frequent low frequency, long duration tectonic tremor activities and other SSEs during the interseismic period. Better understanding of SSEs can provide constraints on stress transfer and loading of the locked fault that may lead to earthquakes during an earthquake cycle.

Seismic studies link SSEs to high interstitial fluid pressure. However, how high pore pressure impedes fault propagation is unknown. We conducted deformation experiments to investigate how slip events along gouge bearing faults transform from slow to fast and back as pressure conditions change. A layer of fine-grained quartz gouge was placed between the saw-cut surfaces in porous sandstone samples that were subject to conventional triaxial loading. By changing the confinements and/or pore pressures, our deformation experiments produced different slip events, from dynamic, audible stick-slip to slow, silent slip. Our data show that under the same pore pressure, increasing effective pressure produces larger dynamic stick-slip events. However, there exists a threshold (~100MPa for the fined-grained quartz gouge used in this study) beyond which stick-slip events are prohibited and creep takes place. In contrast, under the same effective confinement, increasing pore fluid pressure causes a transition from stick-slip to slow-slip in the same fault. Based on the experimental results, we propose a synoptic view of rock strengths and the slip instability as a function of depth and pore fluid pressures.

Acknowledgement: This work is supported by DE-FG02-07ER15916: Evolution of Pore Structure and Permeability of Rocks Under Hydrothermal Conditions, PI: Wenlu Zhu

Recent publications (2016-present, *student, ^postdoc):

1. *Xing, T. and Zhu, W. (2019) Pressure Dials to Tune Slip Events between Slow and Fast, to be submitted to Nature Geosciences.
2. *Xing, T. Zhu, W., French, M., and Belzer, B. (2019) Stabilizing Effect of High Pore Fluid Pressure on Slip Behaviors of Gouge-bearing Faults, *Journal of Geophysical Research*, in revision.
3. *Xing, T., Zhu, W., Fusseis, F., and Lisabeth, H. (2018) Generating porosity during olivine carbonation via dissolution channels and expansion cracks, *Solid Earth*, https://doi.org/10.5194/se-9-879-2018.
4. *Lisabeth, H., Zhu, W., Xing, T., De Andrade, V. (2017) Dissolution assisted pattern formation during olivine carbonation, *Geophysical Research Letters*, doi: 10.1002/2017GL074393.
5. *Lisabeth, H., Zhu, W., Kelemen, P., Ilgen, A. (2017) Experimental evidence for chemo-mechanical coupling during carbon mineralization in ultramafic rocks, *Earth and Planetary Science Letters*., doi:10.1016/j.epsl.2017.06.045.
6. Zhu, W., Fusseis, F., Lisabeth, H., Xing, T., Xiao, X., De Andrade, V., Karato, S. (2016) Experimental evidence of reaction-induced fracturing during olivine carbonation, *Geophysical Research Letters*, doi: 10.1002/2016GL070834.
7. *Miller, K., Zhu, W., Montesi, L, Gaetani, G., Le Roux, V., Xiao, X. (2016), Experimental evidence for lithologic melt partitioning between olivine and orthopyroxene in partially molten harzburgite, *Journal of Geophysical Research*, doi: 10.1002/2016JB013122.
8. ^French, M. E., Zhu, W., *Banker, J. (2016), Fault slip controlled by stress path and fluid pressurization rate, *Geophysical Research Letters*, 43, doi:10.

Figure: Stick-slip events as a function of Left) confinement Pc; Right) pore fluid pressure Pf.